University of Calgary

PRISM Repository **https://prism.ucalgary.ca**

The Vault Open Theses and Dissertations

2016

Compact Optical Sensing Systems for pH and Other Substances Detection - Theory and Implementation

Cao, Muyun

Cao, M. (2016). Compact Optical Sensing Systems for pH and Other Substances Detection - Theory and Implementation (Master's thesis, University of Calgary, Calgary, Canada). Retrieved from https://prism.ucalgary.ca. doi:10.11575/PRISM/25367

http://hdl.handle.net/11023/3020

Downloaded from PRISM Repository, University of Calgary

UNIVERSITY OF CALGARY

Compact Optical Sensing Systems for pH and Other Substances Detection - Theory and Implementation

by

Muyun Cao

A THESIS

SUBMITTED TO THE FACULTY OF GRADUATE STUDIES

IN PARTIAL FULFILMENT OF THE REQUIREMENTS FOR THE

DEGREE OF MASTER OF SCIENCE

GRADUATE PROGRAM IN ELECTRICAL ENGINEERING

CALGARY, ALBERTA

MAY, 2016

© Muyun Cao 2016

Abstract

Chemical detection is of importance in research and industry. Optical sensors based on contact imaging realize the chemical detection in compact, efficient and inexpensive ways. In the first project real-time optical pH sensor based on complementary metal–oxide–semiconductor (CMOS) contact imaging and microfluidics, an optical contact imaging sensor for pH detection with capillary microfluidics is proposed. The CMOS array detects the changes of light intensity after absorption by phenol red doped sol-gel filters while the level of absorbance corresponds to a pH value of the analyte. Deposition methods of sol-gel are optimized and compared. In the second project, real-time optical concentration sensor based on Raman scattering, CMOS contact imaging is presented. This biochemical optical sensor is designed for detecting the concentration of solutions. It is built with a laser diode, an optical filter, a sample holder and a commercial CMOS sensor.

Acknowledgements

This work could not be finished without the support from my supervisor. First and foremost, I would like to acknowledge my supervisor Dr. Yadid-Pecht with University of Calgary for offering me the opportunity to work in Integrated Intelligent Sensing (I2Sense) Lab. With her guidance, I managed to finish these meaningful projects. Thanks to her trust and support, my research, reading and writing abilities are practiced and enhanced. Also thanks to Dr. Murari with University of Calgary for his support and advice during my graduate study. Thanks to F. Hickley with machine shop for providing this work with technique support. Thanks to Dr. Dalton with Advanced Micro/nanosystems Integration Facility (AMIF) in University of Calgary for training me with spin coating facilities. Thanks to Dr. J. Ronsky and A. Boyle with Zymetrix for providing advance working space and fume hood for this work.

Also thanks to the I2Sense lab members for the great research atmosphere. Thanks to my family and friends.

Table of Contents

Abstract····ii

Acknowledgements····iii

Table of Contents····iv

List of Tables····vii

List of Figures and Illustrations····viii

List of Symbols, Abbreviations and Nomenclature····ix

CHAPTER 1 INTRODUCTION····1

1.1 Aims····1

1.1.1 Detect the Liquid's pH Value in Real-Time····1

Method····1

Approach····1

Expected result····2

1.1.2 Utilize Raman Scattering Principle to Detect Chemical Properties in Liquid2

Method····2

Approach····2

Expected result····3

1.2 Summary of Contributions····3

1.3 Organization of the Dissertation····4

CHAPTER 2 Optical pH Sensor Based on CMOS Contact Imaging and Microfluidics····6

2.1 Background of pH Detection····6

2.1.1 Importance and Usage of pH Detection····6

2.1.2 Traditional pH detection Methodologies····6

2.2 Optical pH Detection Methodologies·····8
2.2.1 Optical pH Detection Systems·····8
2.2.2 Optical pH Sensors Reviews·····9
2.2.2.1 Absorption Based Optical pH Sensors Reviews·····9
2.2.2.2 Fluorescence-Based Optical pH Sensor Reviews·····11
2.2.3 Contact pH Imaging System Components and Methods·····12
2.2.3.1 Introduction to the CMOS Sensor in Use·····13
2.2.3.2 Introduction to Contact Imaging·····14
2.2.4 Dye-Mediated pH Optical Filter·····15
2.2.4.1 Important Properties of Probes and Matrix·····15
2.2.4.2 Matrix of Filters·····15
2.2.4.3 Phenol Red·····16
2.2.4.4 Deposition Method·····17
2.2.4.5 Micro Printing Method·····19
2.2.4.6 Microfluidics·····22
2.3 The System Structure, Build-Up, and Optimization·····22
2.3.1 Build Microfluidics on CMOS Sensor Board·····24
2.3.2 Sol-gel Filter Preparation·····26
2.3.3 Bond Enhancement between Sol-Gel and Surface·····28
2.3.4 Appearance and Reduction of Sol-Gel Cracks·····28
2.3.5 Optimization of Coating and Printing Methods·····29
2.3.5.1 PVAc Linking Layer·····29
2.3.5.2 Microcontact Printing of sol-gel·····29

2.3.5.3 Screen and Spin Printing Method of Sol-Gel·····31
2.4 Experiments, Data, and Analysis·····34
2.5 Comparison with Other Optical pH Sensors·····37
2.6 Applications·····40
CHAPTER 3 REAL-TIME BIOCHEMICAL SENSOR BASED ON RAMAN SCATTERING WITH CMOS CONTACT IMAGING ·····41
3.1 Background of Raman Scattering and Spectroscopy·····41
3.1.1 Introduction to Raman Scattering·····41
3.1.2 Introduction to Raman Spectroscopy·····41
3.2 Reviews of Compact Raman Systems·····43
3.3 System Design·····44
3.3.1 Concentration Detection Principle·····44
3.3.2 System Setup·····46
3.4 Experiments and Results·····48
3.4.1 Experiments setup·····48
3.4.2 Results·····50
CHAPTER 4 CONCLUSIONS AND FUTURE DIRECTIONS ·····51
4.1 Optical pH Sensor Based on CMOS Contact Imaging and Microfluidics·····51
4.1.1 Future Work·····51
4.2 Real-Time Biochemical Sensor Based On Raman Scattering with CMOS Contact Imaging·····52
4.2.1 Future Work·····52
Reference·····53

List of Tables

Table 1 Phenol Red Doped Sol-Gel Solutions..... 27

Table 2 Phenol Red Doped Sol-Gel Filters Properties 27

Table 3 Statistics of Intensities of CMOS Images of Forward pH Test 4- 12..... 36

Table 4 Statistics of Intensities of CMOS Images of Reverse pH Test 12- 4..... 38

Table 5 Comparison with Other Optical pH Sensors..... 39

List of Figures and Illustrations

Figure 2.1 Full-range Optical pH Sensor Array 10

Figure 2.2 PDMS Microfluidic Device 11

Figure 2.3 System Structure 13

Figure 2.4 Absorption Spectrum of Phenol Red (a) in Sol–Gel Glass Film and (b) in Buffer Solution (After [8]) 17

Figure 2.5 Dip Coating 18

Figure 2.6 (a) PDMS Stamp (b)-(d) Failure Events of Micro Contact Printing 20

Figure 2.7 Screen Printing 21

Figure 2.8 Sketch of the pH Optical Sensor with Microfluidics 22

Figure 2.9 3D Printed Mold (a) Part One and (b) Part Two 23

Figure 2.10 Capillary Microfluidics on CMOS Sensor Board 25

Figure 2.11 (a) Large Volume Related to the Velocity of Sol (b) Fixed Volume Related to the Thickness of Sol Coating 30

Figure 2.12 (a) Ultrathin Glass Mask (b) Screen-Spin Coating Sol-Gel Pattern 32

Figure 2.13 (a) Failure Case 1 Edge Effect, (b) Failure Case 2 Detached, (c) Punched From Top and Back 33

Figure 2.14 (a) Plot of Intensity-pH in Forward Test (1) and Jump Test (3) (b) Plot of Intensity-pH in Reverse Test (2) and Jump Test (5) (c) Plot of Intensity-Number Jump Test (5) (d) Plot of Intensity-Temperature Test (6) 35

Figure 2.15 CMOS Images Analysis 37

Figure 3.15 Absorption Spectrum of the Rayleigh Filter 46

Figure 3.16 Schematic of the System (Not in Scale) 47

Figure 3.17 Experimental Setup for Comparison with Spectrometer Results (Not in Scale) 47

Figure 3.18 Averaged Spectrums of Raman Peaks of Sodium Chloride Solution from 0.2 M to 4.0 M by Step of 0.2 M 49

Figure 3.19 Averaged Intensity Values of CMOS Sensor Outputs 49

List of Symbols, Abbreviations and Nomenclature

Symbol	Definition
pH	Negative logarithmic of hydrogen ion concentration
pKa	Acid dissociation constant
Vo	Lifting speed in dip coating
t90	Time taken for the signal to achieve 90% of the Final value
A	Absorption
ε	Molar absorptivity
l	Thickness
c	Molar concentration

Abbreviations	Definition
CMOS	Complementary metal–oxide–semiconductor
PVAc	Polyvinyl acetate
EMBC	Engineering in medicine and biology society
ISFET	Ion selective field effect transistor
MOS	Complementary metal–oxide–semiconductor
PCP	Purple cabbage pigment
OLEDs	Organic light-emitting diodes
PVC	Polyvinyl chloride
PAni	Polyaniline
PDMS	Polydimethylsiloxane
HPTS	1-hydroxypyrene-3,6,8-trisulfonic acid
SNAFL	Seminaphthofluorescein
GERD	Gastroesophageal reflux disease
Sol	Sol-gel solution
Gel	Sol-gel in gel status
BPR	Bromopyrogallol red
LED	Light-emitting diodes
TEOS	Tetraethoxysilane
SAMs	Self-assembled monolayers
LSI	Large-scale integration
CW	Continuous wave
CCD	Charge-coupled device
SPAD	Single photon avalanche detector
HeNe	Helium neon
AOTF	Acoustic-optic tunable filter
OD	Optical density
DI	Deionized
UV	Ultraviolet
Laser	Light amplification by stimulated emission of radiation

CHAPTER 1

INTRODUCTION

The goal of this research is to design and create low cost and compact systems for chemical detection. This chapter states the aims of the work including the approaches and results. This thesis is organized as described in this chapter.

1.1 Aims

This thesis consists of two aims.

1.1.1 Detect the Liquid's pH Value in Real-Time

Method:

Phenol red is a pH sensing probe which changes optical properties according to the pH value it interacts with. A sensing film made from phenol red and sol-gel is able to change the chemical information into optical information. Sol-gel acts as the matrix of the sensing filter which entraps the indicator and dries it down from liquid status to a porous solid structure which allows the interaction of the probe with the sample poured on it. Polyvinyl acetate (PVAc) acts as a linking layer which helps the bonding and reusability. Capillary microfluidics is involved in giving real time flowing in and flow out as well as precise readouts. The contact imaging system benefits from the high light collecting efficiency compared to bulky optical systems with discrete lenses.

Approach:

The CMOS sensing array detects the changes of light intensity by the absorption of phenol red doped sol-gel filter whose optical density and absorption spectra vary corresponding to the pH value in the sample. The image signals are processed by image processing software to compare the intensities to database values to obtain the exact pH value. Deposition methods of sol-gel are compared and a spin coating screening printing process is proposed for sol-gel specific pattern

creation. Two identical Phenol Red doped sol-gel filters are printed on the CMOS sensor and their readout values are averaged to get more precise results.

Expected Result:

Achieve a compact pH sensor with a detecting range of pH 4 to 12 with an accuracy of 1 in 15 seconds with this system. The resolution can be increased by increasing the response time.

1.1.2 Utilize Raman Scattering Principle to Detect Chemical Properties in Liquid.

Method:

Raman spectroscopy is an effective tool for both qualitative and quantitative chemical characterization and identification for biology and medicine. The intensities of total Raman scattering are related to the concentrations of the same chemicals. A highly sensitive CMOS sensor is able to detect Raman scattering passing through an emission filter which blocks overall Rayleigh scattering.

Approach:

A miniature measurement set-up which utilizes a commercial CMOS imaging detector to determine the overall intensity of the Raman scattered photons with respect to the concentration of the sodium chloride solution sample is presented. The system is built with a laser diode, an optical filter, a sample holder, and a commercial CMOS sensor. The output of the system is analyzed by an image processing program. The excitation source of this Raman system is a 532 nm laser diode that illuminates the sample plane at a 90 ° incidence angle. An absorption filter attached to the CMOS imaging sensor blocks the Rayleigh scattering.

Expected Result:

The spectra and CMOS images of Raman signals are compared and results show that the chemical concentration of the samples can be detected by this proposed sensor. The system provides instant measurements with a resolution of 0.2 to 0.4 M.

1.2 Summary of Contributions

A qualitative chemical detection sensor for bio-medical solutions was designed. These sensor readings were compared to spectrometer readings by detecting sodium chloride solutions from 0.2 M to 4 M with 0.2 M step. The experiments were done with control to make sure the amount of Raman scattering photons received by the spectrometer and by the CMOS sensor are approximately the same. The experiment results showed a non-linear relation between the concentrations of sodium chloride solution and the total Raman scattering intensity. This relation was confirmed by literature [1, 2]. So with the database of intensity-concentration for known chemicals solution, this real-time biochemical sensor based on Raman scattering with a CMOS contact imager was able to give the concentration in 8 seconds with a resolution of 0.4 M and in 2 minutes with a resolution of 0.2 M. This was presented in IEEE Engineering in Medicine and Biology Society (EMBC), 2015.

Two sensing filters together with high shape, thickness and response repeatability on a CMOS sensing array were created. Based entirely on contact imaging techniques, using a CMOS sensor board makes this system more compact than other optical pH sensors based on the electrical diodes and spectrometers. The system represented a miniaturized pH detection device, with low power consumption. This device was inexpensive to fabricate and environmentally friendly. The sensing components presented in this system were easy to remove, and thus, facilitate reuse of the sensor while the embedded diode system is not reusable. The microfluidics was applied to

enable the system to be proficient enough for online monitoring. Sol-gel deposition and printing methods were optimized so that a thin crack-free sol-gel pattern can be printed without the use of an expensive inkjet and spray material printer. A repeatable screen-spin printing method that was promising for the successful printing of sol-gel based thin patterns was proposed. The low-cost compact system, exploiting the benefits of contact imaging and sol-gel technology, with accurate measurement of pH values ranging from 4 to 12 by a resolution of 1 in 15 seconds in 20^{o}C to 40^{o}C environments. This work was presented in IEEE Sensors Journal, 2015.

1.3 Organization of the Dissertation

This thesis is organized as follows: in chapter 1 section1.1, the rationales, approaches and expected results of this thesis are listed. In section 1.2, the contributions of this work are summarized.

In chapter 2 section 2.1, the motivation of a miniaturized real-time optical pH sensor with wide detection range and low cost is proposed. The background study of modern optical pH filters including absorption and fluorescence probe-based are reviewed. In section 2.2, contact imaging system components are briefly introduced such as a CMOS sensor, contact imaging system build-up, reagent-mediated pH optical filter. Moreover, properties of sol-gel matrix and a probe "phenol red" are presented. In section 2.3, deposition and printing methods of the sol-gel matrix are compared in order to obtain thin, crack-free and uniform sol-gel patterns on CMOS sensors in a laboratory environment. The contact optical pH detection system with capillary microfluidics is revealed. This section contains the system build-up structure, the designs of large-scale integrated (LSI) microfluidics and LSI capillary microfluidics, printing of sol-gel patterns by spin coating and microcontact printing methods. The implementations and experimental procedures are highlighted for phenol red doped sol-gel filter preparation and

optimization of the filter thickness by calibrating the parameters in the printing methods. In section 2.4, the experimental data and analysis of this system are presented. Comparative data analysis revealing the stability, reversibility and resolution is presented. In section 2.5, this pH sensor is compared with other optical pH sensors. In section 2.6, some applications of this pH sensor proposed.

In chapter 3 section 3.1, the background of Raman scattering and Raman spectroscopy is introduced. In section 3.2, other works on compact Raman systems are reviewed. In section 3.3, the design of the system based on Raman scattering is presented. In Section 3.4, the experiments preparation and setup, and the methods to process the data and the comparison of this biochemical sensor to spectrometer are introduced.

In chapter 4, the conclusions and future work of the two projects are presented in section 4.1 and section 4.2.

CHAPTER 2

OPTICAL PH SENSOR BASED ON CMOS CONTACT IMAGING AND MICROFLUIDICS

2.1 Background of pH Detection

In chemistry, pH is a numeric scale used to specify the acidity or basicity of an aqueous solution. It is the negative of the log base 10 of the concentration of the active hydrogen ions or H^+ in units of moles per liter. Solutions with a pH less than 7 are acidic and solutions with a pH greater than 7 are alkaline or basic. To monitor and control pH value in industry, laboratory and everyday life, there are some traditional pH meters available in the market.

pH is a key parameter in many areas, for instance, environmental monitoring, biomedical diagnostics, life sciences and pharmaceutical research, marine and soil examination, food processing, cosmetics etc.

2.1.1 Importance and Usage of pH Detection

The enzyme reactions in the food and beverage products require pH motoring, because the action of enzymes is affected by pH. Each food has an optimum pH value [1]. Medical organizations measure pH to adjust reagents. They also measure the pH of body fluids, such as blood, gastric juices and urine, for medical research, medical testing, and treatment. Researchers at dental colleges measure pH when studying tooth decay [2].

2.1.2 Traditional pH Detection Methodologies

pH strips are based on pH indicator dyes which are covalently attached to a reagent paper. The color of the dyes changes according to pH. To use the pH strips to measure the pH of a liquid, immerse the strip in the test solution until color development is complete. The pH value is read

by visual comparison of the color of the testing strips with the color of standard chart. Some universal pH strips consist of a mixture of indicators so there are continuous color changes.

pH strips are the most widely used methods for pH determination in people's daily usage and they are easily accessible on the market. However, pH strips are not able to give a precise, automatic and real-time readout, which limit their usage in laboratories and industries. In contrast, potentiometric pH measurements including glass and non-glass electrodes are widely used.

In potentiometric pH measurements, the potential of an electrochemical cell under pH conditions is measured by the glass or non-glass electrodes. In the case of glass electrodes, the pH-sensitive element is a glass bulb that is fused to a glass tube. The tube is filled with natural potassium chloride solution and contains a silver-silver chloride wire that forms the electrical connection. The reference system is located in the outer glass tube which also consists of potassium chloride solution and silver-silver chloride wire. A junction protects the reference wire from being physically connected to the solution to be measured without stopping the electrical connection between them. When the pH electrode is immersed in the solution for detection, the hydrogen ions are able to penetrate the boundary area of the membrane outside of the glass bulb- gel layer while other larger ions remain in the solution, which causes a charge separation. For the natural potassium chloride solution inside the glass bulb, there are fixed numbers of hydrogen ions which penetrate the gel layer inside of the glass bulb. If the pH value inside the bulb differs from the outside, the different amount of hydrogen ions in each gel layer forms a measurable potential difference. The pH value is calculated by measuring the potential difference between the reference wire and the measuring wire. In the case of non-glass electrodes, the pH-sensitive element is an ion selective field effect transistor (ISFET) which uses a Complementary metal–

oxide–semiconductor (MOS) transistor arrangement which contains a pH sensitive layer instead of a metal gate. Positive hydrogen ions forming an excess layer cause the charge to be separated on the other side. As a result, the area between the source and drain become conductive. The resulting current is directly proportional to the pH value in the medium. The reference system is also protected by a junction.

A pH electrode is reliable and easy to operate, has relatively low cost, and facilitates rapid measurement. It also allows for a two-point calibration strategy and shows a wide working range. The disadvantages of the pH electrode include the size, rigid design, and susceptibility to electrical interference and aggressive analytes such as alkaline solutions or fluoride ions which limit its usefulness. They are also mechanically fragile, not suitable for long-term measurements due to electrode signal drift, not well suited for measuring in small sample volumes, and facilitate only single point measurements.

2.2 Optical pH detection Methodologies

2.2.1 Optical pH Detection Systems

An optical pH sensor should be characterized by real-time response, reversibility (result repeatability of forward-low pH to high pH and reversed-high pH to low pH) , reproducibility, temporal or long-term storage (shelf life), operational stability, response time (t90, time taken for the signal to achieve 90% of the final value), sensor resolution (the smallest pH change that a sensor can detect/resolve) in the required pH range, photostability with associated drift, and degree of dye leaching (when dye is not covalently attached to a polymer matrix). In addition, temperature and ionic strength cross-sensitivity should be addressed.

Optical sensors are based on reagents that change their optical properties upon interaction with the analyte of interest. The most commonly measured optical properties are absorption,

fluorescence intensity, and decay time, but in addition, reflectance, refractive index, light scattering, and light polarization have also been used as analytical parameters. The reagents are dissolved in some kind of matrix to be solidified to a layer [3].

Many books and review papers have been published where advantages and disadvantages of optical chemical sensors, as well as recent developments in the field, have been discussed [4-8].

2.2.2 Optical pH Sensors Reviews

pH optical sensing filters use pH sensitive probes whose optical properties change when pH environment varies. The optical properties can be color, transparency and fluorescence intensity. The optical pH sensors can be classified into absorption based and fluorescence-based sensors which are reviewed separately in the following. The pH probes are dissolved in a certain matrix such as sol-gel and polymers which will be a solid transparent layer to capsulize the probe with a porous structure. The hydronium ions will diffuse into the pores then interact with the probe to change the optical properties. Polymer and Sol-gel are most widely used to make optical filters due to their flexibility, and mechanical and chemical stability.

2.2.2.1 Absorption Based Optical pH Sensors Reviews

Classical absorption-based pH sensor operation is based on a color change of a sensor layer in which a pH indicator dye is encapsulated. Examples of such dyes include phenol red, bromocresol green, and phenolphthalein. Colorimetric pH sensors using neutral red and a mixture of malachite green oxalate and bromocresol green have also been reported [4].

Chen et al. published an optical pH sensing sol-gel film entrapped purple cabbage pigment (PCP) as pH indicator dip-coated onto glass slides. Measurements by ultraviolet–visible spectrophotometer and p-polarized reflectance were shown suggesting a response between pH 2.0 and 11.0 with linear calibration, but no good reversible results were reached from pH 7.0 to

11.0. The response time is 2 minutes [9]. Yari and Dinarvand published a similar sensor film employing the indicator dye bromopyrogallol red (BPR) in sol-gel. It reported a pH detection range of 2.33-9.42 in one minute [10].

A portable optical multianalyte pH sensor array was presented by Martinez-Olmos et al. [4] consisting of 12 organic light-emitting diodes (OLEDs) display as a programmable light source, 12 different drop-coated pH sensing channels as a colorimetric sensor array, and an array of 12 digital color detectors. As shown Figure 2.1[4]. The 12 different indicators were immobilized in high molecular weight polyvinyl chloride (PVC) polymer layers. Low drift values for both OLED light source and color detectors were measured. A simple algorithm in the microcontroller was to select the sensor output by pH range from 12 detectors. The pH range of the whole device was from pH 0.0 to 14.0 and the resolution of the device was stated as 0.02 pH units, the accuracy as 0.2 pH units, and the response time of 1.5 seconds.

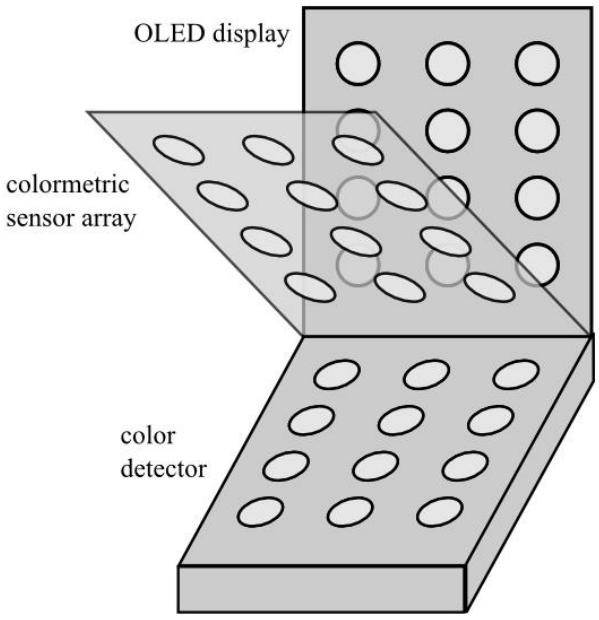

Figure 2.1 Full-range Optical pH Sensor Array

Florea et al. [11] reported a microfluidic device for dynamic pH imaging and mapping with a polyaniline (PAni) coated pH sensitive channel shown in Figure 2.2. The optical properties of the PAni coating changed according to the solution flushed into the Polydimethylsiloxane (PDMS)-based microfluidic device offering continuous colorimetric pH monitoring. The PAni coating was functionalized by flushing the microfluidic channels with oxygen plasma and a solution of N-[3-(trimethoxylsilyl)propyl]aniline. The absorption spectrum of PAni with pH was measured by a spectrometer and showed an increasing absorption at 605 nm and a decreasing absorption at 832 nm with higher pH values. A colorimetric image readout was reported which reflected gradient pH along the microfluidic channel, using a digital camera as the detector.

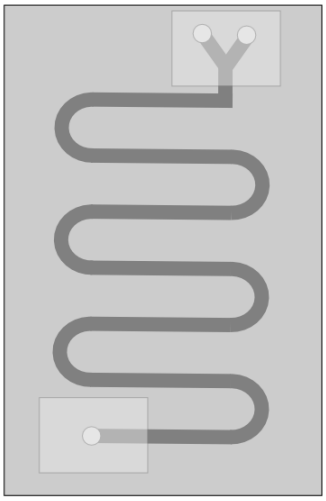

Figure 2.2 PDMS Microfluidic Device

2.2.2.2 Fluorescence-Based Optical pH Sensor Reviews

Fluorescent pH indicators offer better selectivity and sensitivity than absorption-based pH indicators.[5] The most widely used fluorescent pH indicators are 1-hydroxypyrene-3,6,8-trisulfonic acid (HPTS), fluorescein, and derivatives. These dyes usually absorb in the visible

blue region while emission occurs above 500 nm. pH sensors using the seminaphthofluorescein (SNAFL) have also been reported [3].

There has been incremental progress in the field of fluorescence-based optical pH sensors in recent years, mainly in the area of new dyes and dye combinations. Some novel polymer and sol−gel encapsulation matrices have also emerged recently. The most widely used detection method is ratiometric intensity. Normally, fluorescent indicators are less stable than other indicators. However, according to literature, there are fluorescence-based pH sensors that are as stable as absorption-based pH sensors [12-13].

Aigner et al. [6] published a new class of rhodamines pH sensitive indicators employing photoinduced electron transfer. The indicators were covalently immobilized to the sensor matrix. The sensors showed high brightness, good operation stability and high sensitivities in the dynamic range pH 5–7 which was particularly useful for biotechnological applications.

Mintchev et al. published a pH sensor based low-light fluorescence detection for diagnosis of gastroesophageal reflux disease (GERD). pHrodo- a fluorescence-based pH indicator was used due to the properties of biocompatible and hydrophilic. A long hydrophobic tail was chemically added on the pHrodo molecule. The emission intensity increased while pH drops. The matrix to entrap pHrodo was PVAc which was a biocompatible, non-toxic hydrophobic polymer. The sensor was sufficient to detect GERD [14].

2.2.3 Contact pH Imaging System Components and Methods

Based on the literature, an optical contact imaging based pH sensor integrated within a CMOS sensor is created. The probe doped sol-gel solution (Sol) is coated above a commercial sensor to be a pH-sensitive optical filter. In detection, the sample is put on the filter and an excitation light source shines on the sample. The excitation light goes through the sol-gel filter which absorbs

part of the excitation light. The transmission light signal is collected by the CMOS sensor and is transferred to an electric signal to form a picture. Image processing and some algorithms provide analytical results. The optical contact imaging sensor makes the system low cost and miniature. In addition, the optical sensor gives online detection that provides real-time and continuous monitoring. Figure 2.3 shows a basic optical sensor schematic.

2.2.3.1 Introduction to the CMOS Sensor in Use

The CMOS image sensor used in this research is DMM 72BUC02-ML (The Imaging Source). It has a binning model for the improvement of the signal to noise ratio. The sensitivity can be up to 22.4 V/lux-sec if 640 × 480 resolution and 23 frames per second are selected. To pre-treat the sensor board, the M-COAT (liquid silicon glue) is applied all over the sensor board for protection purposes. In contact imaging research the cover glass on sensor boards is often removed to increase light collection efficiency [7] [15]. However, the exposure of the sensing array makes the CMOS and wire bond easily broken. So the cover glass is kept on this research which benefits the stability and long lifetime operation of the sensor in this research.

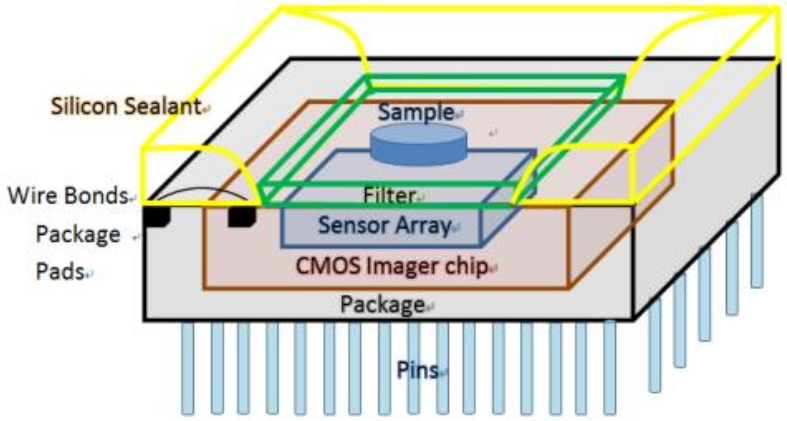

Figure 2.3 System Structure

2.2.3.2 Introduction to Contact Imaging

Contact imaging does not require optical elements, such as lenses, dichroic cubes, optical fibers and path length between the sample and the sensing array, providing better collection efficiency and less optical loss compared to bulk optical systems. In contact imaging [7, 15-17], typically the systems consist of a LED as a light source, a fluorescent indicator selective for the sample of interest and a thin film as an emission filter coated directly on the optical sensor. The objects are in close proximity to the sensor surface and the collection angle of incident light is close to 2π depending on the thickness of the filter. An absorption filter is characterized according to Beer Lambert's Law in equation 2.1.

$$\mathbf{A = \varepsilon l c} \qquad \textbf{(2.1)}$$

Where, ε is the molar absorptivity, l is the thickness of the filter and c is the molar concentration of the absorption dye. Hence, once the absorption dye is chosen, ε is fixed and the two other parameters l and c can be optimized. The thickness and uniformity of the filter play an important role in contact imaging [18-19]. A paper reports that the thickness of an absorption filter with better imaging and good contrast is less than 100 μm [7]. The fluorescence is uniform in all directions, so ideally 50% of emission can be collected by the sensor array. In non-contact imaging [7], because of the long distance between the source and the converging lens, the light collection angle is smaller than the angle in contact imaging.

The high light collection efficiency makes it possible to use a low power light-emitting diodes (LED) as an illumination source for dark objects because the improvement in collection efficiency allows the detection of a weak signal [7]. A LED source has many benefits in general contact imaging systems. LEDs are small scale, low cost and can be integrated with contact

imaging systems. In addition, the LEDs have low excitation energy intensity which reduces photobleaching of fluorescence probes thus the result is more exact.

2.2.4 Dye-Mediated pH Optical Filter

2.2.4.1 Important Properties of Probes and Matrix

The pH sensing matrix should be hydrophilic in order to facilitate proton diffusion and be chemically, mechanically, and thermally stable. Compatibility with a wide range of deposition techniques and cost are also important. The desired features of a pH sensitive dye include an appropriate pKa (negative logarithm of the acid dissociation constant Ka), high absorption ratio and excitation to emission ratio, and a band in the visible region to facilitate the LEDs as low-cost light sources and to minimize photobleaching effects. Fluorescent indicators should also exhibit a large Stokes shift [3] to ease the separation of the emission light from the excitation light.

2.2.4.2 Matrix of Filters

There are three widely used methods for the immobilization of pH indicators in a solid matrix: adsorption, entrapment, and covalent binding. First, adsorption is not reliable, as the dye may easily leach away. Second, entrapment is a relatively straightforward and rapid method to implement. One disadvantage is the possibly slow leaching of the indicator. This problem can be overcome by using indicators in the form of ion-pairs which make them hydrophobic, and therefore, they exhibit poor water solubility. Third, covalent binding is usually complex and time-consuming and needs an appropriate material with a functional group suitable for the immobilization. This method is reliable, as the leaching effects are eliminated. The response of covalently bound indicators is reduced compared to their performance when physically entrapped; optical properties of an indicator may be changed, and pKa shift can also occur [3].

The sol–gel method is a low-temperature process used to synthesize optically transparent, amorphous bulk glasses and thin films either by spin-coating, dip coating or other deposition techniques using organic precursors. It involves a metal alkoxide, water, and a solvent, which are mixed thoroughly to achieve homogeneity on a molecular scale [4].

To make silica glass by this method, a silicon alkoxide such as tetraethoxysilane (TEOS) in the Sol undergoes hydrolysis and condensation at room temperature to produce the gel (a loose network in solid state) [4]. The sol-gel films can be coated onto substrates of planar glass and optical fibers and at Sol for optical chemical sensor applications.

Sol–gel glass, as a supporting matrix, provides a chemically and physically stable environment with optical clarity. The potential usages of sol-gel as indicator phases in optical sensing devices have generated considerable research activity [3, 4].

The traditional alkoxide precursor, TEOS, forms a hydrophobic gel, so the polar probe phenol red has a high risk to leach into the sample in detection. In this work, hydrophilic Ph-triOES is added in TEOS to increase the ability to entrap the polar probes in the Sol [20]. The drawback is the increase of the residue in the porous structure. To overcome this, a thin sensing film is created to achieve a quick response and reduce the residue.

2.2.4.3 Phenol Red

Phenol red exists as a red crystal that is stable in air. A solution of phenol red is used as a pH indicator.

Figure 2.4 (a) [8] shows absorption spectra of phenol red in TEOS/Ph-TriEOS (5%, v/v) sol–gel glass film in buffer solutions of varying pH. From bottom up: pH 5, 6, 7, 8, 9, 10, 11 and 12. Figure 2.4 (b) [8] shows absorption spectra of phenol red in buffer solutions of varying pH. From bottom up: pH 5, 6, 7, 8, 9 and 10. Phenol red concentration: 1.41×10^{-4} M. According to the

absorption spectra, the light source is selected to be 550 nm because the absorption variation is largest at 550 nm.

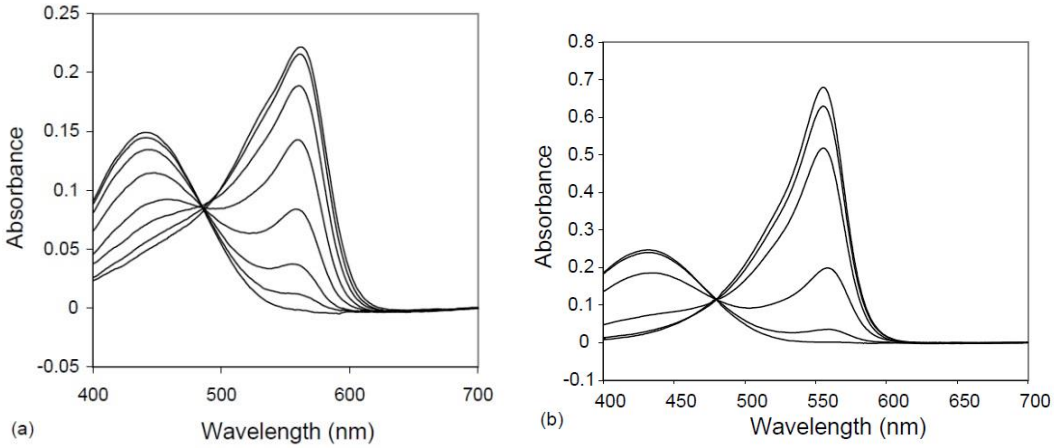

Figure 2.4 Absorption Spectrum of Phenol Red (a) in Sol–Gel Glass Film and (b) in Buffer Solution (After [8])

2.2.4.4 Deposition Method

The solution coating methods are important to make thin uniform layers of optical filters above the CMOS sensing array. Dip-coating and spin-coating are most widely used deposition methods in the laboratory environment and give uniform coating formation. Other techniques include screen printing, spray coating, knife coating, and inkjet or pin printing. Recently, very homogeneous sol−gel-derived films have been achieved using a hemiwicking process [3].

(1) Spin Coating

Spin coating is a procedure used to deposit uniform thin films to flat substrates. It's easy to obtain a layer thickness by adjusting the spin speed. The drawbacks of this method are the existing of comets, striations, chuck marks, edge effects and environmental sensitivity. Comets usually occur when relatively large solid particles impede the normal flow patterns of the solution on the spinning wafer. Striations are radially oriented lines due to the thickness variation in the film caused by non-uniform solvent evaporation. The orientation of striations corresponds

to the direction of major fluid flow. Chuck marks are created by the thermal "communication" between the solution on top of the wafer and the metal vacuum chuck on the back side of the wafer. Wafer edge effects are caused by liquid attached around the entire perimeter due to surface tension and result in thicker coatings in this rim zone. Environmental sensitivity means the ambient environment can affect the coating quality, e.g. the humidity of surrounding air.

(2) Dip Coating

In the dip-coating method in Figure 2.5 [21], the substrate is slowly dipped into a tank containing the sol and is normally withdrawn vertically from the liquid bath at a speed Vo in order to obtain a uniform coating. The moving substrate entrains the liquid in a fluid mechanical boundary layer that splits in two above the liquid bath surface, the outer layer returning to the bath. Since the solvent is evaporating and draining, the fluid film terminates at a well-defined drying line. When the receding drying line velocity equals Vo, the process is a steady state with respect to the liquid bath surface.

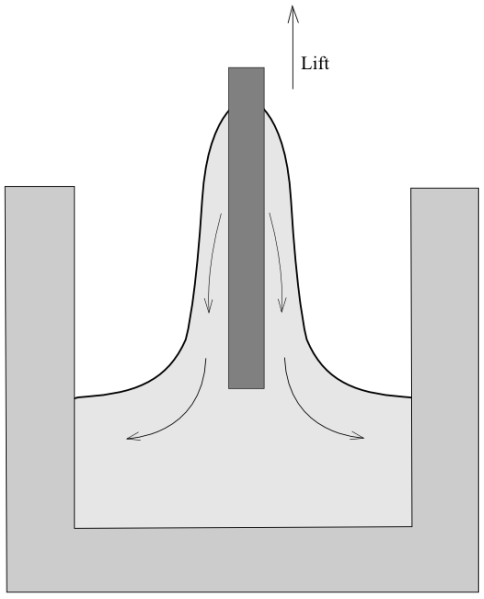

Figure 2.5 Dip Coating

2.2.4.5 Micro Printing Method

The above coating methods are used to make a film above a substrate. The aim of this work is to make a filter array containing several filters which can be used to detect not only pH but also other components and ions in solution. Thus, the printing method is necessary to make small scale patterns above the sensing array.

(1) Microcontact Printing

Microcontact printing is also called nano-transfer printing. It is a form of soft lithography that uses the relief patterns on a master polydimethylsiloxane (PDMS) stamp to form patterns of self-assembled monolayers (SAMs) of ink on the surface of a substrate through conformal contact as in the case of transfer. The first step to print with this method is ink the stamp by immersion and press on the sensing array. The traditional next step is to wait for the ink to dry until no liquid is visible and an ink reservoir is created and then conformal contact the stamp to the substrate to transfer the pattern from the PDMS. The PDMS stamp, in most applications, is a 10:1 weight ratio of silicone elastomer and a silicone elastomer curing agent. The accurate PDMS mold is made by photolithography. As photolithography's cost is high, it contradicts one of our research aims, i.e. low cost, hence mold was not created utilizing photolithography.

The highly hydrophobic PDMS material allows only the use of apolar inks. In this case, sol-gel is hydrophilic in solution status so it can't spread well on the surface. The surface tension makes the sol-gel in a ball shape. The other thing is after the sol-gel drying, it combines very tightly on the PDMS and cannot be printed on the sensing array surface. This may be the reason there are no works reporting sol-gel as microcontact printing ink [22-23].

The solution is to pick up sol-gel in solution status and wait until it transfers to gel status to print because if printed in solution status, the pattern drop will split into two parts and one is

transferred but the other part is left on the stamp. The transferred volume depends on the gelation period. The gel status is a very short intermediate status so it's hard to control. The gelation time depends on the shelf life of sol-gel solution, environment humidity, and temperature. The gelation time can be counted with a timer to get the whole gel film transferred successfully. However, this method is random and not repeatable. The researchers need to be experienced with sol-gel. Also, the pattern is not uniform if not printed in the most appropriate time.

The contact printing stamp is made as follows. Use biopsy punches to cut cured PDMS into 2mm diameter cylinder. Two PDMS cylinders are combined in liquid PDMS and cured shown in Figure 2.6 (a). Because PDMS is flexible, the ratio of height h, width w, and gap distance d need to be carefully chosen to avoid collapse and sagging shown in Figure 2.6 (b) – (d) [23]. The 1.5 mm pace is also to avoid crosstalk of pixels under the filter edge. Three identical filters are printed to average the result to for better reading.

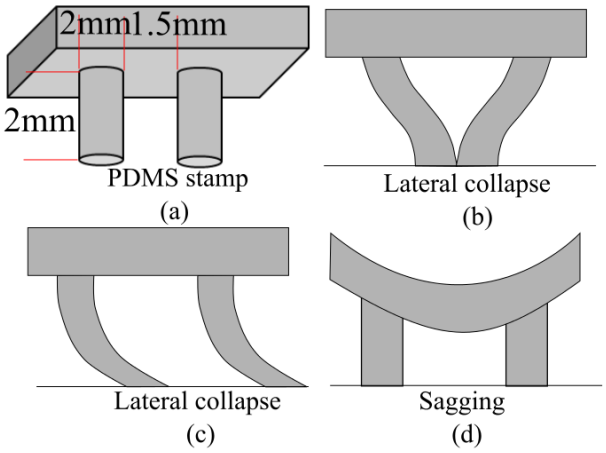

Figure 2.6 (a) PDMS Stamp (b)-(d) Failure Events of Micro Contact Printing

(2) Inkjet Printing

The inkjet printing technique for deposition of materials on paper has attracted attention because the system is rapid, scalable, compatible with paper substrates, and amenable to pattern

formation. As a result, a variety of biomaterials can be deposited on a solid support in a single layer or multiple layers at ambient temperature with relatively low shear rates, with bioactivity being retained for extended periods. Several additives are introduced into ink formulations to optimize the physical properties and to make them stable and ejectable [24]. The most wildly used commercial inkjet printing system is from Fuji Dimatix, which can be used to print many kinds of bio-ink which meet the requirements of viscosity and surface tension. Because of the complex maintenance and high budget of the inkjet printer, although it is common in sol-gel pattern deposition methods used in industry, it's not widely used in laboratories.

(3) Screen Printing

Screen printing is a printing technique that uses a fabric mesh to support an ink-blocking stencil to receive a desired pattern in Figure 2.7 [25]. The attached stencil forms open areas of mesh that transfer ink or other printable materials which can be pressed through the mesh as a sharp-edged image onto a substrate. A fill blade or squeegee is moved across the screen stencil, forcing or pumping ink through the mesh openings to wet the substrate during the squeegee stroke. This process is very suitable for patterning liquid layers in biosensors and is a one step process. However, the resolution is limited to 100μm or even lower.

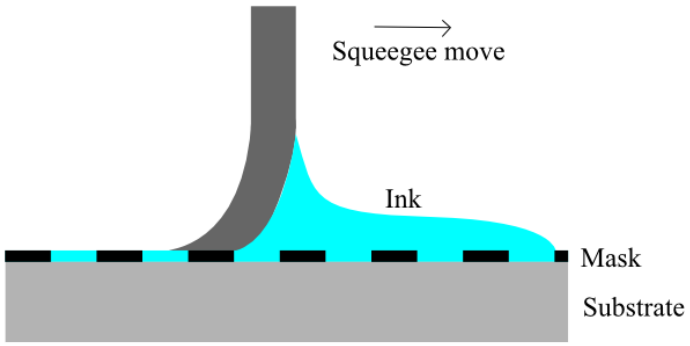

Figure 2.7 Screen Printing

2.2.4.6 Microfluidics

Microfluidics typically refers to fluid flow in man-made channels, not fluid flows in natural microchannels such as blood vessels, plant capillaries. The application area covers from pure analytical chemistry to biology to inkjet printing. Microfluidic large-scale integration (LSI) describes a microfluidic system with channels and chip-integrated microvalves based on flexible membranes. LSI is an easy way to realize laboratory microfluidics [26]. Based on microchannels and control, micropumps, mixers, multiplexers, etc. can be built up with hundreds of units on one single chip [27]. Soft lithography based on the usage of elastomeric stamps makes it possible to fabricate precise PDMS microchannels.

2.3 The System Structure, Build-up, and Optimization

Similarly to the general contact imaging system, the steps of system build up us shown in Figure 2.8. The sensing area of CMOS sensor board in use is 6mm by 7mm. First, the PVAc layer is coated above the sensing array by spin coating. Then two filters are printed above the PVAc layer by screen-spin printing. The whole sensor board and wire bond excluding the sensing array are covered by silicon glue to protect from chemical washes and the analyte.

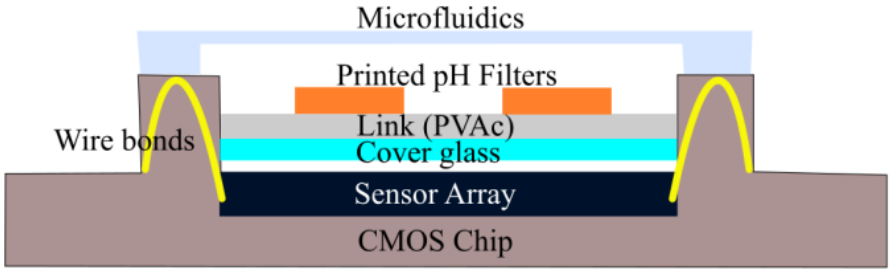

Figure 2.8 Sketch of the pH Optical Sensor with Microfluidics

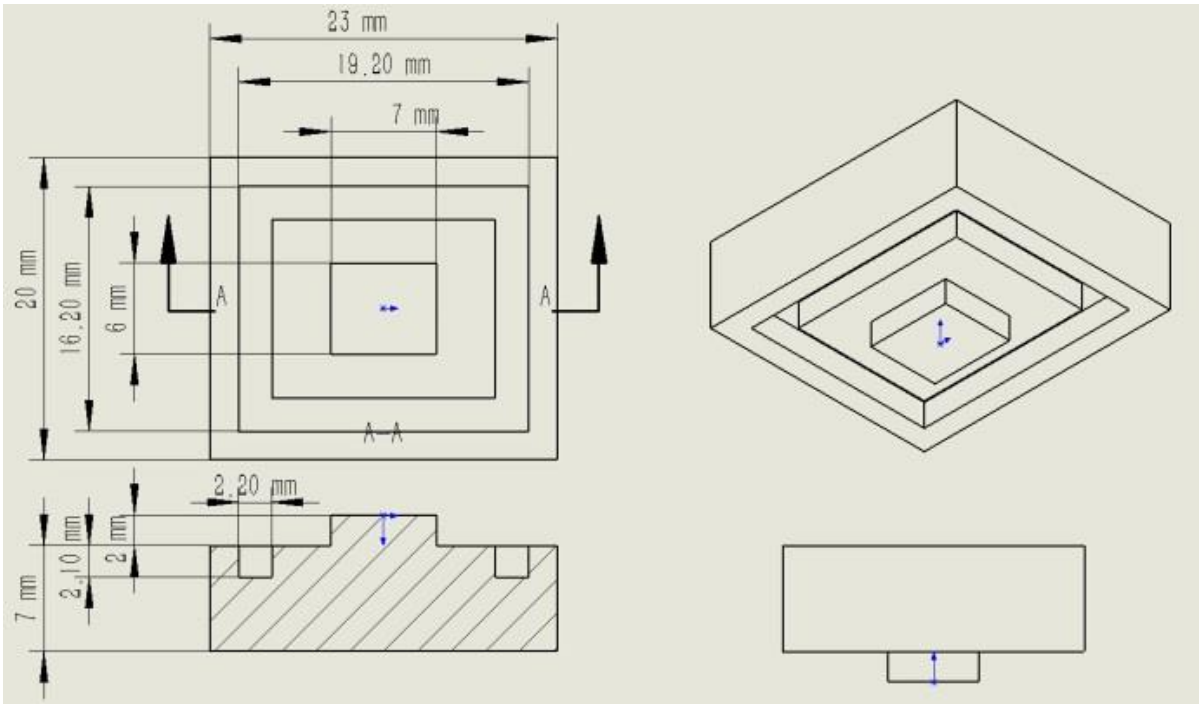

(a)

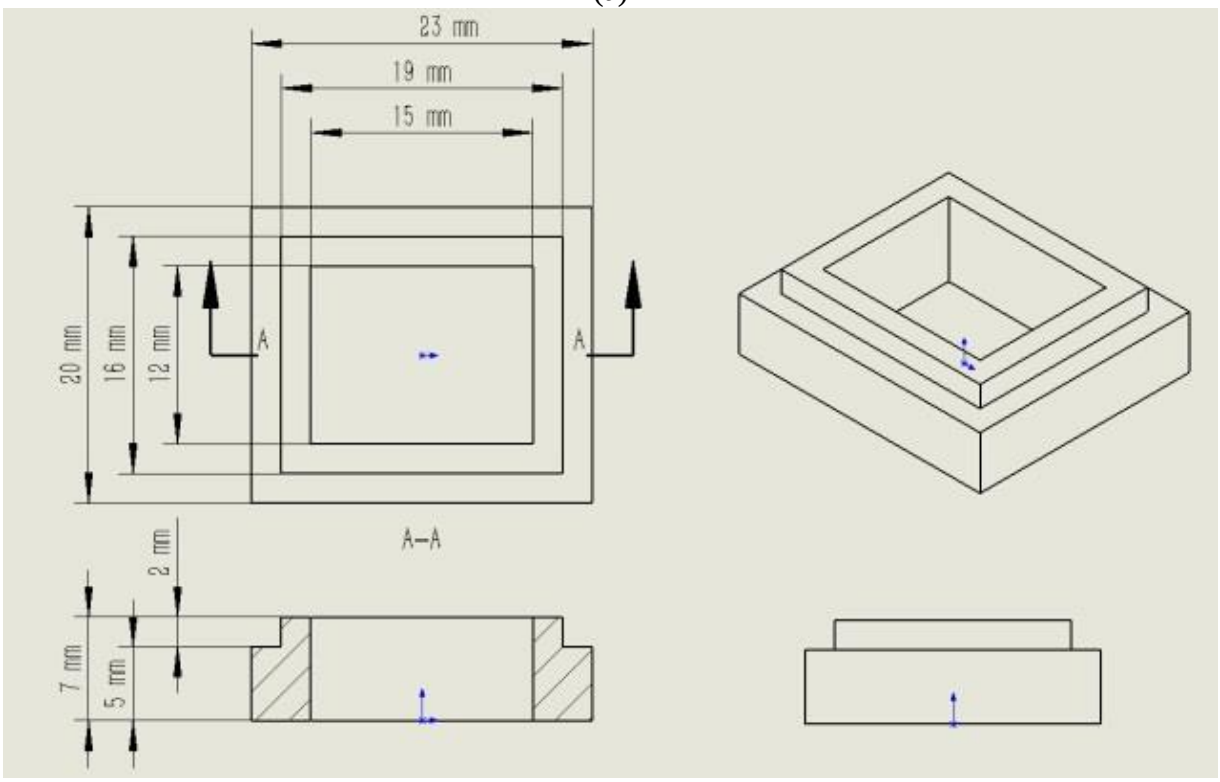

(b)

Figure 2.9 3D Printed Mold (a) Part One and (b) Part Two

2.3.1 Build Microfluidics on CMOS Sensor Board

Large scale integration microfluidics shown in Fig. 2.9 is created in this work. It is used to flow in/ out analyte liquid and fix the volume and the shape of the analyte. The liquid analyte is between the light source and sensing array, so it works as a lens. If the shape of the analyte is different in each test, the different collimation of the penetrating light infects the result. The PDMS chamber is made by a 3D printed mold. The sketch of the mold is drawn with Solidworks shown in Figure 2.9. The 3D printer to be used is a Makerbot Replicator 2X with fused deposition and 100um layer resolution. The fused materials are limited to PLA and ABS. The surface of the 3D printed mold has a weaved structure so it is porous. The design is to make the mold in two parts, part one for the bottom and part two for the wall. Due to the resolution limitation, the mold is made with dimensions shown in Figure 2.9 (a) to be aligned tightly with Figure 2.9 (b) with no leaking and match the sensing array. The bump surface which is attached to the inner top has 0.6 mm polished off to make the surface smooth. To make the chamber body, liquid PDMS is poured into aligned molds and cured on a hot plate overnight. Then the two pieces of molds are separate and the cured chamber body is taken out of the molds. A 1mm biopsy punch is used to punch holes on the chamber and two injectors are used to flow in and flow out analyte. To align the chamber on CMOS sensor board, liquid PDMS is applied above the wire bond and the PDMS chamber is manually pressed on the liquid PDMS. The connection between the silicon glue and PDMS is tight but can be peeled off easily, so remove the chamber and reuse the sensor to print other filters above the sensing array is capable. Despite manual alignment of the position of the three filters and the microfluidics chamber, the detection result is not affected because the volume and shape of the sample is fixed.

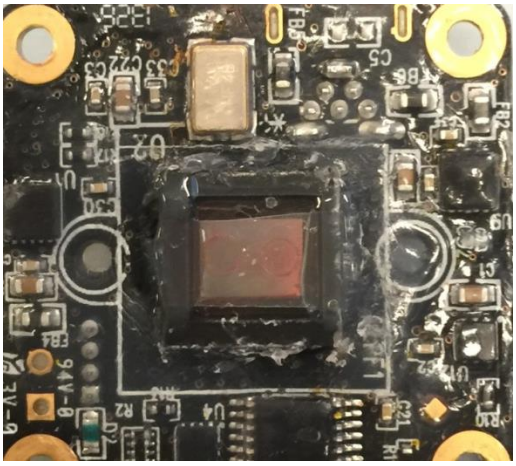

Figure 2.10 Capillary Microfluidics on CMOS Sensor Board

The downsides of this microfluidics design are listed. The holes on the top wall maintain the atmospheric pressure balance. At the same time, the leakage appears at the injector point on the chamber. Moreover, the top wall infects the imaging of the CMOS by causing the picture it takes to have the pattern of the top wall. In addition, the injector cannot extract all the solution in the chamber at one time. To avoid the residue, the chamber needs to be washed by the new solution.

To overcome the shortages, capillary microfluidics which is shown in Figure 2.10 is designed. It's an open room made up of silicon glue and ultra-thin glass. The silicon glue is applied on both narrow sides above the wire bond package. Before the glue dries, press a piece of ultra-thin glass on the silicon glue. A caliper is used to make sure the ultra-thin glass is 0.5 mm. The volume of the room between the ultra-thin glass and the CMOS array is 20 μL. With the transparent and smooth ultra-thin glass and fixed shape and volume of solution, the imaging is under repeatable condition. To flow in the analyte, use a pipette to drop 20 μL of the solution on broadsides close to the CMOS array. The capillarity makes the solution fill the whole room between the ultra-thin glass and the array. To remove the pH solution, a piece of wipe touches the edge of the solution

and all the solution under the cover glass is absorbed. There are no contacts to the filters and no residue is left.

2.3.2 Sol-Gel Filter Preparation

The first step is to acquire the appropriate thickness of the pH filter which is regulated by the ratio of phenol red embedded in sol-gel and the amount of water. The results of different ratio of each component of sol-gel are compared presented in Table 1.

The solutions are spin coated directly on the PVAc link of the same CMOS sensor board. The properties of each sol-gel filter are listed in Table 2with corresponding filter index in Table 1. The picture taken by the CMOS sensor has an 8-bits dynamic range. The setup of the sensor board and light source are kept to be the same. The uniformity and thickness of filters are defined by visual comparison. Solution 1 and solution 2 cannot spread well on the PVAc layer, and form thick filters with cracks upon drying. Solutions 3- 6 form thin uniform filters without cracks. The response means that the intensity value is fixed after response time. The deviation of the mean value of pH 12 to 4 determines the resolution of the filter. For solution 1 and 2, the sol-gel layer is thick and the picture is dark. Solutions 5 and 6 have low concentrations of TEOS and phTEOS, so the filters are thinner than filters 4 and 5. They have less phenol red probes so the pictures are bright.

As a conclusion from Table 1 and Table 2, the thinner filters offer shorter response times whereas the thicker filters show longer response times. Considering the fact that the larger deviation in TABLE II is better, filter 4 is found best and solution 4 is selected for further experiments.

Further steps are taken to achieve crack-free filters as following: spin coating of the Sol 4 at 1000 rpm on PVAc linker followed by baking the sensor board on a hot plate maintained at 60^{o}C

for 30 minutes. By heating, the stress value of sol-gel decreases [28], so the thickness of the sol-gel filter is significantly influenced during the fabrication process. Here the optimized filter 7 is obtained, which is the finalized optimum filter in this system.

Table 1 Phenol Red Doped Sol-Gel Solutions

	TEOS/ mL	Ph-TEOS/uL	HCl(0.1m/L)/mL	Water/ mL	Phenol Red/mg	Phenol Red (mg/ml)
Solution 1[8]	4	200	1.6	5	10	0.9
Solution 2	4	200	1.6	5	13	1.3
Solution 3	4	200	1.6	10	14	0.9
Solution 4	4	200	1.6	10	20	1.3
Solution 5	4	200	1.6	15	19	0.9
Solution 6	4	200	1.6	15	27	1.3

Table 2 Phenol Red Doped Sol-Gel Filters Properties

	Spread uniformity	Thickness	Cracking	Response time /second	Mean value of pH 10	Mean value of pH4	Deviation between pH 4 and 10
Filter 1	Poor	Thick	Yes	500	36	119	83
Filter 2	Poor	Thick	Yes	1000	25	97	72
Filter 3	Good	Thin	No	20	48	156	108
Filter 4	Good	Thin	No	15	55	177	122
Filter 5	Good	Thin	No	15	165	244	79
Filter 6	Good	Thin	No	10	130	225	95

2.3.3 Bond enhancement between sol-gel and surface

Because of the hydrophobicity of the sol-gel glass film and the silicon surface, the bond between them is loose. If sol-gel is coated and dried at room temperature, numerous cracks are generally formed followed by a partial separation of the sol-gel film from the silicon or glass substrate. Also, when the pH solution is applied, the sol-gel filter tends to cast off easily.

A PVAc layer is a possible link to bond sol-gel to the sensing array firmly, but this additional layer results in edge effects on the array because the PVAc layer is spin coated. In addition, the thickness of the PVAc layer reduces light collection efficiency of CMOS sensor. The other solution is thermal bonding at 60 ℃. The process is to dry the sol-gel pattern at 60 ℃ for 12 to 48 hours. A Si-O-Si bond is expected to be formed between the sol-gel and Si_3N_4 of the sensing array [18-19].

The thermal bonding of sol-gel is tested as following. The sol-gel layer is loosely adhered to the cover glass and heated at 60 ℃ for 48 hours to create a Si-Si bond. The result shows that the Si-Si bond is strong; the sol-gel coating tends to attach firmly to the cover glass, even washed by pH solutions ranging from pH 4 to12. Experiments, however, reveal that the Si-Si bond cannot be broken without damaging the cover glass of the CMOS sensor. As a result, the sol-gel layer is not detachable and the sensor is not reusable. So this bond enhancement method cannot be applied in the case of this system. Therefore, the PVAc layer works as a linker above the sensing array.

2.3.4 Appearance and Reduction of Sol-Gel Cracks

The thick sol-gel patterns crack firstly at the edges which dry quicker than other parts. The cracks then keep growing towards the centers of the patterns forming branch shapes.

Theoretically, cracks appear from drying stress. As the film dries, it shrinks in volume. Once the film is attached to the substrate and unable to shrink uniformly in all directions, the reduction in volume is compensated completely by a reduction in thickness. When the film has solidified and stresses can no longer be relieved by flow, tensile stresses develop in the plane of the substrate. Strategies to avoid cracking include increasing the fracture toughness of the film, reducing the volume fraction of solvent at the solidification point and reducing the film thickness. In the cases of organic polymer films, plasticizers are often added to reduce the stiffness of the film and thus avoid cracking [28].

The properties of sol-gel vary a lot in the shear time, concentration, temperature and humidity [28, 32]. All the data regarding printing methods represent the first day of sol-gel preparation at a room temperature and humidity if not stated.

2.3.5 Optimization of Coating and Printing Methods

2.3.5.1 PVAc Linking Layer

The PVAc coating can be created uniformly by spin-coating [33] and is found to adhere to both the cover glass and the sol-gel. It comes off by washing with acetone. In this case, a PVAc coating works as a linker between the sol-gel layer and the cover glass. It helps the uniform spreading and attachment of the sol-gel. The thickness of a coated layer is adjusted by the viscosity of the PVAc solution and the spin speed.

2.3.5.2 Microcontact Printing of Sol-Gel

The PDMS stamp is the most widely used mold for micro-printing due to ease in shaping and compatibility to most chemicals. In this research, the PDMS mold is made as shown in Figure 2.6 (a). Two PDMS cylinders are created by punching 2 mm high solid PDMS pieces with 2 mm a biopsy punch. The two cylinders are aligned and cured in liquid PDMS base in petri-dish.

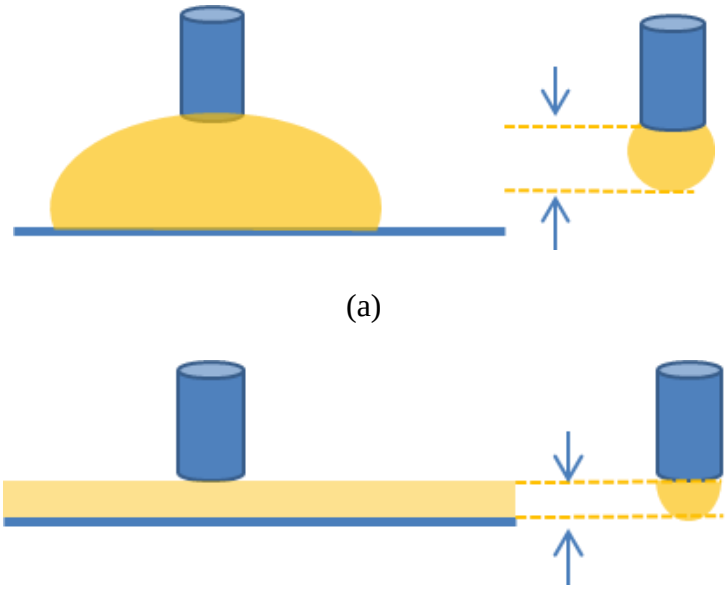

(a)

(b)

Figure 2.11 (a) Large Volume Related to the Velocity of Sol (b) Fixed Volume Related to the Thickness of Sol Coating

Printing in the gel state makes the pattern nonuniform. Figure 2.11 (a) shows that if the Sol is picked up from a drop directly, the volume being picked up is too much and makes the pattern too thick. To create a pattern thin enough and to avoid cracks, once the Sol is picked up by the stamp, it is repeatedly used for printing. The fifth patterns are found crack-free and remain of the same thickness. A set of fifth spots is observed under a microscope and results reveal that they are uniformly printed with similar thickness. However, this process is manual, cannot be quantified and offers variability in the patterns especially when different people perform the process. In addition, the fifth patterns are too thin and contain deficient probes while the fourth patterns are thick with cracks. Figure 2.11 (b) shows if the Sol is picked up from a spin coated Sol layer, the thickness of a picked up layer is generally fixed. In the aim of picking up a thin crack-free layer, the spin speed is required to be high. However, Sol undergoes gelation in a

short time after or during spin coating because the airflow in the spinner accelerates the gelation. Consequently, the coated filters are dry by the time the coating is finished and therefore cannot be picked up anymore.

PVAc is used to make a hydrophilic stamp. Sol spreads well on the PVAc stamp and the volume picked up is less than the PDMS stamp. However, PVAc is not compatible with Sol. In conclusion, microcontact printing is not suitable for sol-gel.

2.3.5.3 Screen and Spin Printing Method of Sol-Gel

The first step of this method is like the general screen printing. A piece of ultra-thin glass with two punched 2 mm diameter holes is used as a mask. The mask can be attached tightly to the CMOS array with PVAc coating and removed easily, as shown in Figure 2.12 (a). The Sol is poured on the ultra-thin glass screen which was already attached to the CMOS array. It flowed well on the hydrophilic surface and entered into the holes. A piece of cover glass is used as a squeegee to slide it on top of the mask as Figure 2.7. The thickness of the ultrathin glass is 20 μm, so the sol-gel pattern dried at room temperature in about 10 μm. The sol-gel spots contain cracks because they are thick. Therefore, the spin-coating method is combined with an ultra-thin glass screen in order to decrease the thickness as the second step. Following the above steps, the sensor board is spun in the spinner. At a high spin speed, the patterns are thin, uniform, and crack-free as Figure 2.12 (b). The screen-printing spin-coating process is repeatable in terms of the materials to be printed, like sol-gel and polymer, thickness and uniformity between each printed pattern.

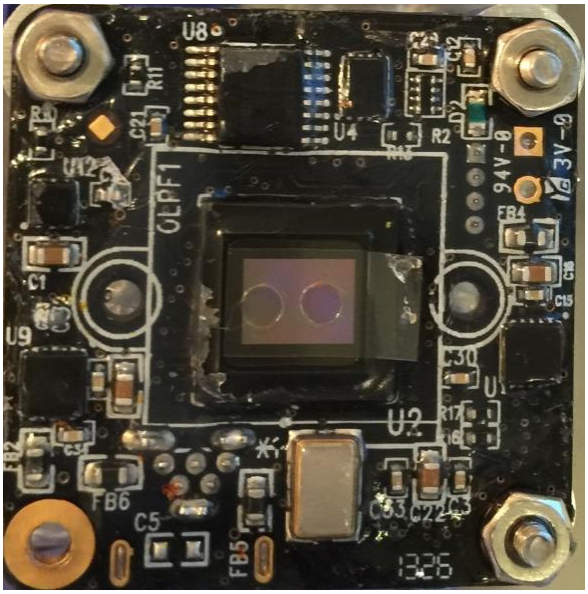

(a)

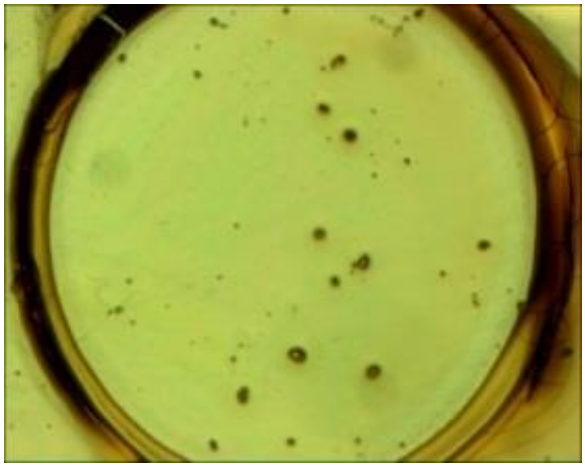

(b)

Figure 2.12 (a) Ultrathin Glass Mask (b) Screen-Spin Coating Sol-Gel Pattern

The concern with this process is that the two surfaces of the ultra-thin glass mask are not flat because the edge of the holes are convex on the penetrated side and concave on the punched side as shown in Figure 2.12 (a) and (b). First, if the ultra-thin glass mask is attached to the PVAc layer on the CMOS array as shown in Figure 2.13 (a), the convex edge of the punched holes

increases the edge effect during spin coating. Second, if the ultra-thin glass mask is attached to the PVAc layer on the CMOS array as shown in Figure 2.13 (b), the concave edge of the punched holes makes the ultra-thin glass not attach tightly. The solution is to punch on both sides slightly as shown in Figure 2.13 (c) while not penetrating the ultra-thin cover glass completely to the other side.

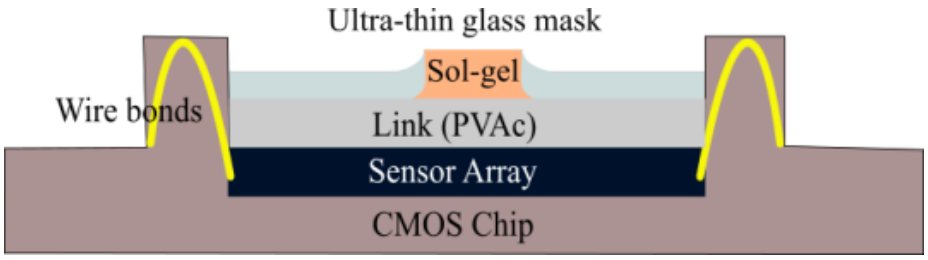

(a)

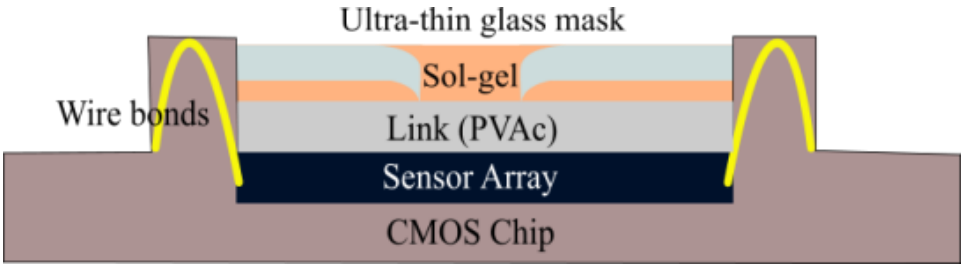

(b)

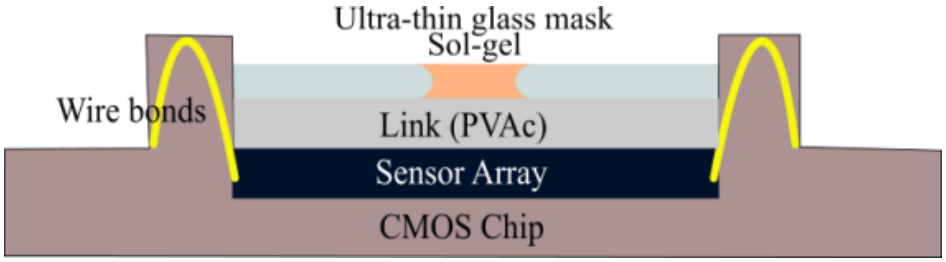

(c)

Figure 2.13 (a) Failure Case 1 Edge Effect, (b) Failure Case 2 Detached, (c) Punched From Top and Back

2.4 Experiments, Data, and Analysis

In this section, the data are collected from filter 7 as described in section 2.3.2. Each test is done with 550 nm LED light source by injecting a 20 μL sample into the capillary microfluidics on this pH optical detection system. No ambient light is received by the CMOS sensor. Pictures are taken by a CMOS sensor after 15 seconds. The images are analyzed by an imaging processing software to obtain the intensity and the values of two identical filters and averaged.

The samples in this study are standard pH solutions with pH values of 4, 5, 6, 7, 8, 9, 10, 11, and 12, respectively. 20 μL samples are injected next to the capillary microfluidics and are absorbed into the microfluidics. To remove the sample, a piece of swipe soaks the the remaining sample by touching the edge of the microfluidics. A set of tests are performed: (1) going through pH 4 to pH 12 sequentially (forward), (2) pH 12 to pH 4 (reverse) sequentially, (3) jump test pH 4 to pH 7 to pH 10, (4) jump test pH 10 to pH 7 to pH 4, (5) random jump test, (6) temperature tests. Each test is repeated10 times and the intensity of the stable CMOS sensor images are plotted in the graphs. The statistics of intensities of CMOS images for the ten repeated tests are listed in Table 3 and Table 4. The plots of filter density-pH value are shown in Figure 2.14 (a) to (d). The unit of Y-axis intensity means the value of an 8-bit CMOS imager which has a maximum value of 255 and a minimum value of 0. From Figure 2.14 (a) and (b), there are no overlaps of intensities of each pH value and that a maximum resolution of pH value 1 is achieved. In the pH range from 6 to 9, a resolution which is smaller than one is revealed. But due to the limitation of standard pH solutions in this research, this resolution is not reported in this paper. The trends of forward and reverse are the same. According to Figure 2.14 (c), the pH value of each test can be observed by the CMOS sensor output. The temperature of the sensor, sol-gel filter, and pH

solution increases from 20 ^{o}C to 40 ^{o}C due to the functional heat of the CMOS sensor board itself.

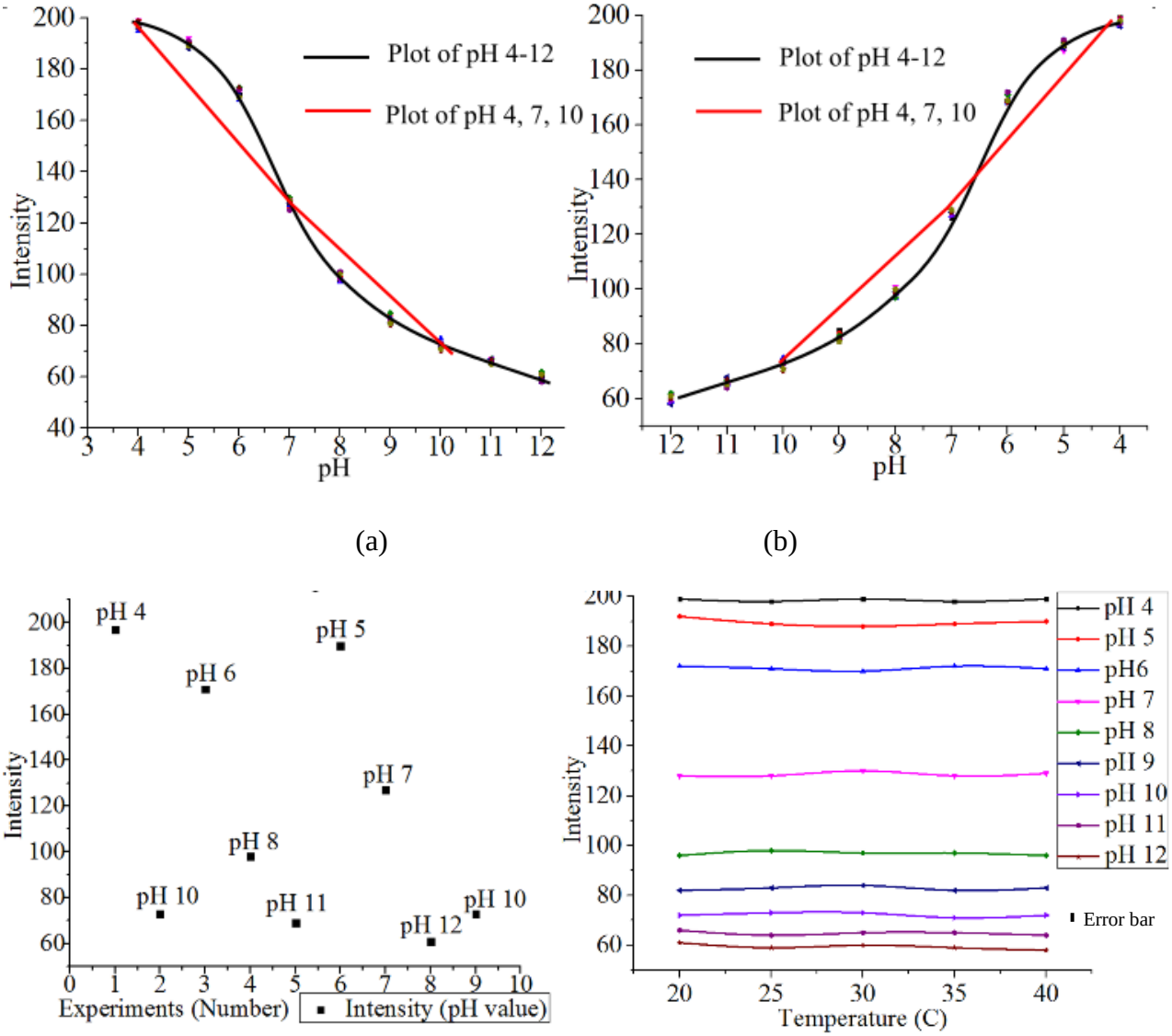

Figure 2.14 (a) Plot of Intensity-pH in Forward Test (1) and Jump Test (3) (b) Plot of Intensity-pH in Reverse Test (2) and Jump Test (5) (c) Plot of Intensity-Number Jump Test (5) (d) Plot of Intensity-Temperature Test (6)

From Figure 2.14 (d), the intensity of each pH value does not change with varying temperature.

As a conclusion, this optical contact imaging sensor for pH detection is able to detect pH ranging from 4 to 12 randomly in 15 seconds at a temperature ranging between 20 ^{o}C to 40 ^{o}C.

If the response time is increased to 150 seconds by averaging 10 15 seconds readout, the resolution can be increased to lower then 1. This is the tradeoff between response time and resolution.

Table 3 Statistics of Intensities of CMOS Images of Forward pH Test 4- 12

Intensity / pH	Max Intensity	Minima	Range	Mean	Standard Deviation	Deviation/Range (Percentage)
4	198	195	3	196.5	1.2	40.0
5	191	188	3	189.9	1.1	36.7
6	173	168	5	170.5	1.7	34.0
7	130	125	5	127.9	1.4	28.0
8	101	97	4	99	1.3	32.5
9	85	80	5	82.2	1.4	28.0
10	75	70	5	72	1.3	26.0
11	65	67	2	66	0.9	45.0
12	61	59	2	59.8	1.2	60

Figure 2.15 shows the method to analyze the CMOS images of this pH sensor. The images captured by the CMOS of pH tests from 4 to 12 are stacked in ImageJ (National Institutes of Health). A circle is drawn on each filter and the software reads and averages all the pixels in this circle from each image. The results are recorded and plot in OriginLab (OriginLab Corporation).

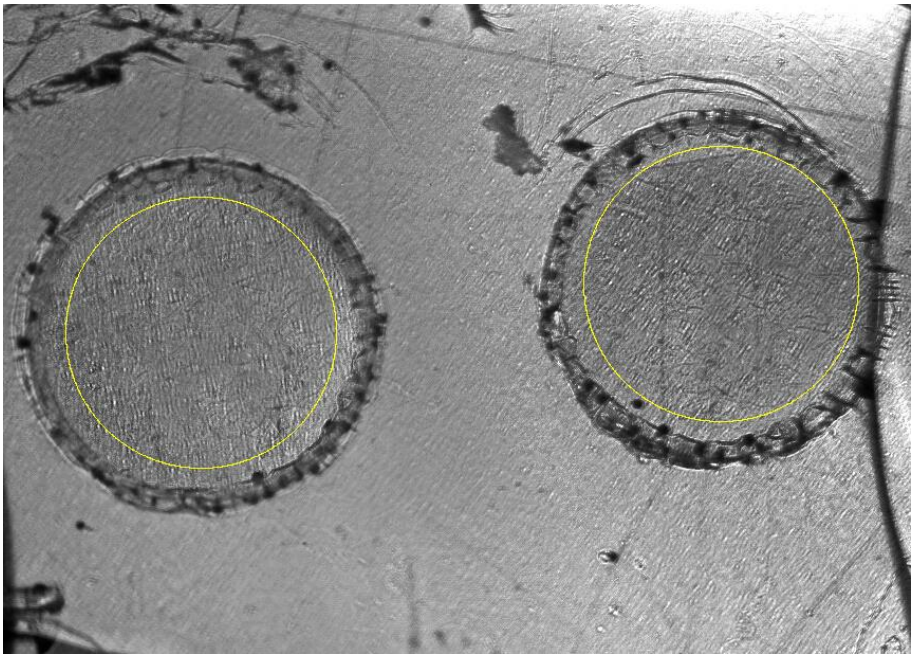

Figure 2.15 CMOS Images Analysis

2.5 Comparison with Other Optical pH Sensors

Compared to the full-range pH sensor published by Martinez-Olmos et al. [4], a CMOS imaging sensor replaced their twelve photodiodes to simplify the system and make it more robust. The CMOS sensor is reusable and only one LED is needed as the light source. This reduces the cost of the system and is research and environment-friendly. However, the detection range of this work is between pH 4 to pH 12 with a resolution of 1, which is comparatively narrower than that work. Compared to planar pH sensors [10], this work reports a wider range of detection, i.e. between pH 4 to pH 12, with excellent reversibility and good response time. Compared with the microfluidics-based pH sensors [11] that use external Raman and scanning electron microscopy to analyze the image of the sensor, the CMOS imager with integrated microfluidics facilitates the realization of a compact and portable lab-on-a-chip system for pH detection. Details are shown

in Table 5 in which room temperature refers to 20^{o}C. Total costs and dimensions of the systems are assumed based on their chemicals, materials, electronics etc.

Table 4 Statistics of Intensities of CMOS Images of Reverse pH Test 12- 4

Intensity / pH	Maxima	Minima	Range	Mean	Standard Deviation	Deviation/Range (Percentage)
12	61	59	2	60.1	1.3	65.0
11	67	64	3	65.8	1.2	40.0
10	75	70	5	72.4	1.4	28.0
9	85	81	4	82.5	1.2	30
8	101	97	4	98.9	1.2	30
7	129	126	3	128	1.4	46.7
6	172	168	4	169.9	1.5	37.5
5	190	187	3	189.4	1.2	40
4	199	196	3	197.9	1.3	43

Table 5 Comparison with Other Optical pH Sensors

	This work	Mintchev et al.[14]	Florea et al.[11]	Yari [10]	Chen et al.[9]	Martinez-Olmos et al.[4]
pH detection range	4-12	1-7	2-8	2-10	2-7	0-14
Resoluti-on	1	1	1	1	1	0.02
Respons-e time/s	15	N/A	N/A	60	120	1.5
Reusabi-lity	Yes	No	No	Yes	Yes	No
Real time	Yes	No	Yes	No	No	No
Temperatu re Range	20-40 ^{o}C	Room	Room	Room	Room	Room
Imaging system	Yes	Yes	No	No	No	Yes
Dimensio ns /cm	4×3×4	3×3×3	7×4×0.5	N/A	N/A	15×17×5
Total Cost/ US dollar	300	700	700	200	300	800

2.6 Applications

The novelty of this pH sensor is short response time, temperature stability and automatic pH recording, water resistance, reusability, miniaturization and low-cost. This system provides a continuous feedback other than discrete point-to-point off-line sampling. The applications of this system can be but is not limited to real-time monitoring such as sewage disposal treatment, environmental pollution monitoring, aquatic cultivation and other pH changes in water. With a water resistant silicon glue protected sensor board, cable and LED, the optical biosensor can be submerged into water. This sensor is especially suitable for miniaturized and low-cost applications are home aid, for instance, pH detection for cosmetics and skin care products for people with sensitive skin, bread fermentation control and dental care for saliva pH measurements to maintain pH value above 5.5.

CHAPTER 3

REAL-TIME BIOCHEMICAL SENSOR BASED ON RAMAN SCATTERING WITH CMOS CONTACT IMAGING

3.1 Background of Raman Scattering and Spectroscopy

Raman scattering is the effect of inelastic scattering of a photon. It is possible to observe molecular vibrations by an inelastic scattering process, thereby learning the structure of molecules and distinguishing contaminants in mixtures.

3.1.1 Introduction to Raman Scattering

Raman and Rayleigh scattering happen at the same time. When a light beam impinges on molecules, interactions of elastic collisions and inelastic collisions will happen. On one hand, in elastic collisions, there is no energy exchange between the photons and the molecules. The direction of movement will change but the frequency will be the same. This kind of scattering is called Rayleigh scattering with the intensity of about 10% of the incident light. On the other hand, in inelastic collisions, there is energy exchange between the photons and the molecules. The photons change their moving directions, vibration and rotation frequency by getting energy from, or losing energy to molecules. This kind of scattering is defined as Raman scattering with the intensity of 10^{-7} to 10^{-8} of incident light and happens in 10^{-12} to 10^{-13} seconds after the incidence. Based on this phenomenon, different molecules will have a corresponding Raman spectrum due to having different molecular bonds.

3.1.2 Introduction to Raman Spectroscopy

Raman spectroscopy is an effective tool for both qualitative and quantitative chemical characterization and identification for biology and medicine [34]. For a qualitative measurement,

a Raman spectrum profile provides a unique chemical fingerprint. The qualitative measurements are used to identify and distinguish materials, such as to analyze the components of chemical solutions in biomedical areas. For a quantitative measurement, the concentration of the active ingredients in the solution is usually directly proportional to the intensity of the Raman scattering peaks. The qualitative measurements are used to identify the concentration of solutions with known ingredients, such as specific buffer solutions in biomedical experiments, and biologically cultivated products. The aim is to build a compact label-free and real-time low-cost system based on quantitative Raman scattering. The measurements of the system should be accurate, precise and repeatable.

The light source for illuminating the sample to excite Raman scattering is a continuous wave (CW) laser operating in the visible, near-infrared or near-ultraviolet range [35-37]. The molecular vibrations and rotations in the sample are changed by the laser excitation, resulting in the energy (wavelength) of the scattered photons being shifted up or down (anti-Stokes or Stokes scattering) in emitted wavelengths.

A high-sensitivity photonic sensor is necessary to detect Raman scattering because the main difficulty of Raman measurement is separating the weak Raman scattered light from the intense Rayleigh scattered light. Raman spectrometers typically use holographic diffraction gratings and multiple dispersion stages to achieve a high degree of laser rejection. This makes the Raman instrument bulky, challenging to operate, and expensive. Additionally, since spontaneous Raman scattering is very low in intensity, traditional Raman spectrometers typically use scientific grade, back thinned charge-coupled device (CCD) arrays as the detector because of the higher quantum efficiency, higher resolution and larger available dynamic range compared to CMOS. Recently, however, researchers demonstrated the application of CMOS single photon avalanche detector

(SPAD) in Raman measurement [37], fluorescence suppression [38] and high-speed measurement [39].

Based on previous research, designing this Raman scattering system with CMOS contact imaging is preferred. The Integrated Intelligent Sensing (I2Sense previously ISIS) Lab at the University of Calgary developed lens-free fluorescence contact imaging sensor with a CMOS for neuron-monitoring [15] and chemical detection in water [7, 15-17]. The contact imaging does not require optical elements, such as lenses, dichroic cubes, optical fibers and path length between the sample and the sensing array, providing better collection efficiency and less optical loss compared to bulk optical systems [7, 15-17]. In this Raman scattering based optical system, contact imaging is applied to avoid extra loss and obtain the most of the Raman scattering signal.

In this study, a miniature measurement set-up is presented which utilizes a commercial CMOS imaging detector to determine the overall intensity of the Raman scattered photons with respect to the concentration of the sodium chloride solution sample. The excitation source of this Raman system is a 532 nm laser diode that illuminates the sample plane at 90° incidence angle. An absorption filter attached to the CMOS imaging sensor blocks the Rayleigh scattering. Spectra measurements are obtained by using QE Pro spectrometer (Ocean Optics) [40]. The data of spectrums and CMOS images are compared and results show that the chemical concentration of the solution can be detected by this sensor.

3.2 Reviews of Compact Raman Systems

Dou et.al [41] published a highly sensitive, compact Raman system without a spectrometer for quantitative analysis of biological samples. The system was built with a semiconductor laser, spherical integration type of cell-holder, Raman shift bandpass filter, photodiode, multi-meter and personal computer. This system was not able to provide Raman spectra because it did not

have a spectrometer. It was used to assume the intensity of a particular Raman band, for instance quantitative analysis of a particular sample. They applied this system to determine the concentrations of glucose and acetone in urine containing glucose and/or acetone artificially.

Cullum et.al [42] reported a lightweight, self-contained, field portable Raman instrument for a quick real-time detection of primary mixture components. The system utilized a helium neon (HeNe) laser for excitation, an acoustic-optic tunable filter (AOTF) for wavelength discrimination, and an avalanche photodiode for detection. Both solids and liquids samples were analyzed (both solids and liquids) using this instrument for the evaluation of parameters such as spectral resolution, sensitivity, and data acquisition speed for certain environmentally important compounds. The results of these measurements were compared with the results of a commercial Raman system.

3.3 System Design

3.3.1 Concentration Detection Principle

The principle of using a CMOS sensor to detect the concentration based on Raman scattering is explained in this section. In a solution, Rayleigh scattering intensity does not do an effective job of verifying the concentration of samples. However, Raman scattering is selective to specific molecules and by evaluating the peaks of Raman spectrum, the ingredients and concentration of the sample can be known [43]. By excluding the Rayleigh scattering, the photons that impinge the CMOS sensor are from Raman scattering and are proportional to the concentration of the solution. The system consists of a light source, an optical filter, a solution sample, and a CMOS sensor. Their properties are decided according to the following description.

The wavelength of the laser is fixed to 532 nm in this sensor. Rayleigh scattering intensity is proportional to the negative fourth power of the excitation wavelength [43]. When detecting

solution concentration, the water absorption requires consideration. The electromagnetic radiation absorption of liquid pure water in the 300 nm to 700 nm visible range is presented in [44]. The lowest absorption which is about 2% lies in the 400nm to 600nm range. Higher absorption which is greater than 28% appears in wavelengths which are greater than 700 nm. So in order to exclude interference of H_2O molecules and increase Raman scattering intensity compared to near infra-red excitation, the light source wavelength should be in the range of 400 nm ~ 600 nm. In this work, a 50mW high-power 532 nm laser with the collimated beam diameter of 1.2 mm is used as the excitation source.

Detecting the concentration by the CMOS sensor requires to totally exclude the Rayleigh scattering in this system with an absorption filter. The Rayleigh scattering is random in all directions, so high angle selective interference filter cannot be used. Because the Rayleigh scattering is 10^6~10^7 time stronger than the Raman scattering [39], the absorption filter with the optical density (OD) of >7 and a sharp transmission slope as shown in Figure 3.15 is used in this system. This optical filter blocks photons of a wavelength which are shorter than 550 nm from Rayleigh scattering. The CMOS sensor receives the Raman scattering photons from 550 nm to 700 nm.

The solution sample in this study is sodium chloride solution because the solution is easy to be prepared in a wide range of concentration. Considering the O–H stretching in sodium solution, the peaks of different concentration shifts a little bit and the shift is non-linear [43-44]. The sample of interest which is sodium chloride solutions is prepared from 0.1 M to 4 M with the step of 0.2 M by dissolving corresponding grams of sodium chloride in deionized (DI) water.

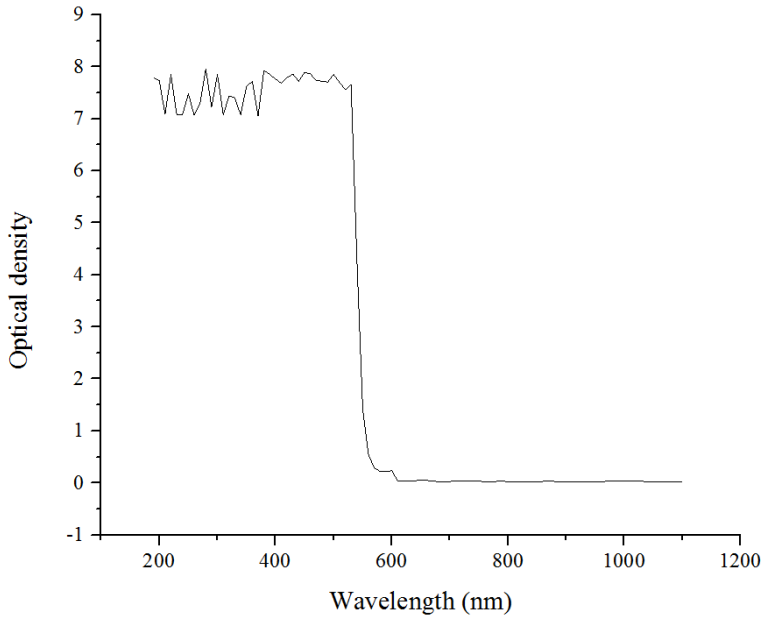

Figure 3.15 Absorption Spectrum of the Rayleigh Filter

3.3.2 System Setup

The Raman scattering based CMOS imaging system used in this study is shown schematically in Figure 3.16. Raman scattering was excited by a 50mW high-power 532 nm laser diode with the collimated beam diameter of 1.2 mm. An ultraviolet (UV) fused quartz cuvette with four polished sides which are transparent and has no Raman emission contains the solution sample. The laser is glued on one side of the cuvette and the absorption filter attached CMOS sensor is glued on the adjacent side of the cuvette.

For comparing measurements, the same absorption filter is attached between the cuvette and the optical fiber coupler as shown in Fig. 3. The Raman photons were coupled into a spectrometer by an optical fiber with 1000 μm diameter core on the opposite side of the CMOS sensor. The Raman scattering photons pass through the absorption filters and directly impinge on the CMOS imaging sensor and an optical fiber of the spectrometer. The Raman scattering light is uniform in all directions. So the Raman signal observed at 90 ° by the CMOS sensor and at -90 ° by the

spectrometer to the laser beam are the same. A piece of laser absorption material is attached opposite to the laser. The silicon glue is used to attach and cover the laser, cuvette, filter and CMOS sensor for contact imaging and biocompatibility.

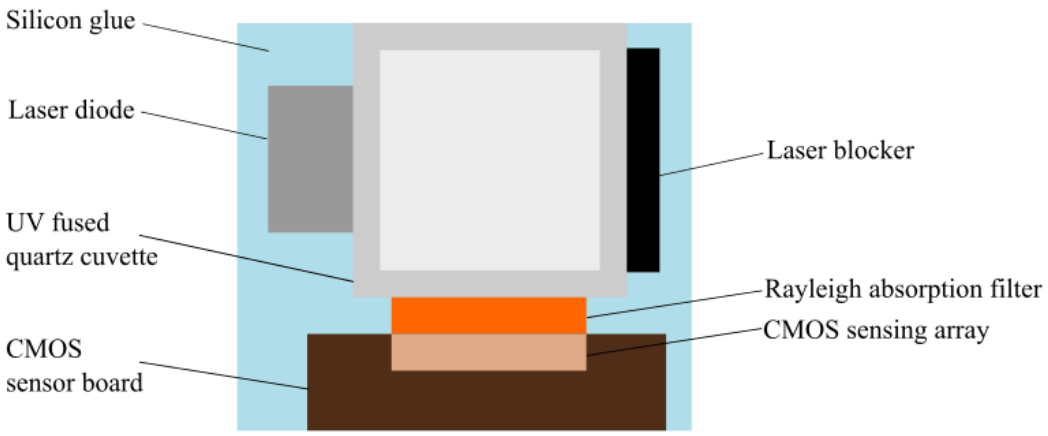

Figure 3.16 Schematic of the System (Not in Scale)

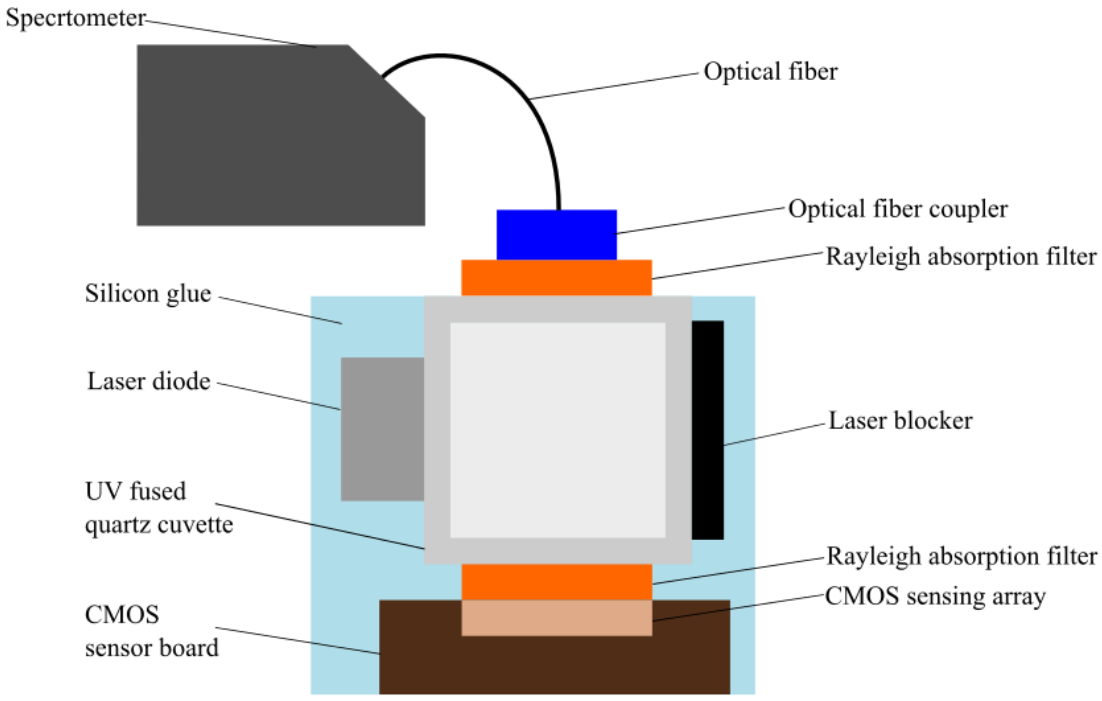

Figure 3.17 Experimental Setup for Comparison with Spectrometer Results (Not in Scale)

The properties of the computer software for the spectrometer and CMOS sensor are adjusted carefully. For the spectrometer, the integration time is set to be 8 seconds to get a strong Raman scattering signal. For the CMOS sensor, the gain is13; the integration time is 8 seconds; and the gamma is 160. With the settings, the intensity value of the CMOS sensor for 0.2 M is 151 and for 4 M is 204. With these settings, the dynamic range of the output intensity is largest. The signal of the CMOS sensor output is processed by an image processing program to analyze the intensity which is comparable to the spectrum within the detection range of the CMOS sensor.

3.4 Experiments and Results

3.4.1 Experiments Setup

The sodium chloride solutions are tested from 0.1 M to 4.0 M with the step of 0.2 M with the system shown in Figure 3.18. Each concentration is tested 10 times by the spectrometer and the CMOS sensor. The values of the spectra are averaged on every sampling wavelength. The output image files from the CMOS sensor are averaged for every pixel on every image. The averaged spectrums of solutions are shown in Figure 3.18 and the averaged CMOS sensor output intensity is shown in Figure 3.19.

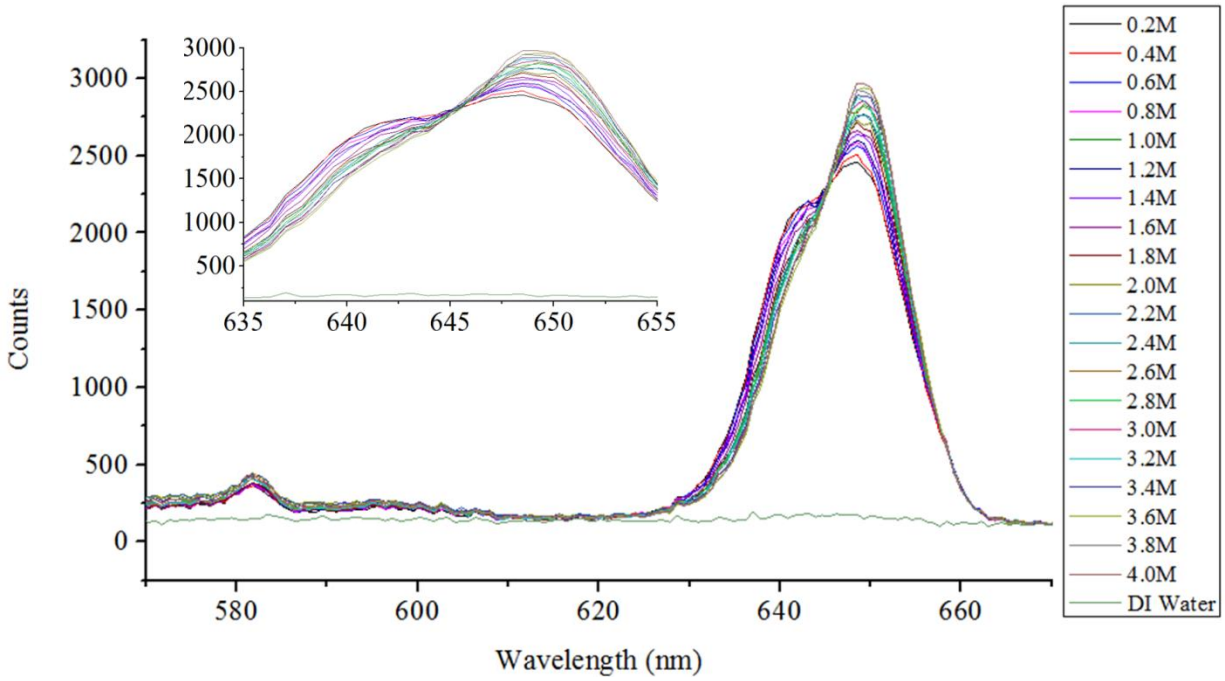

Figure 3.18 Averaged Spectrums of Raman Peaks of Sodium Chloride Solution from 0.2 M to 4.0 M by Step of 0.2 M

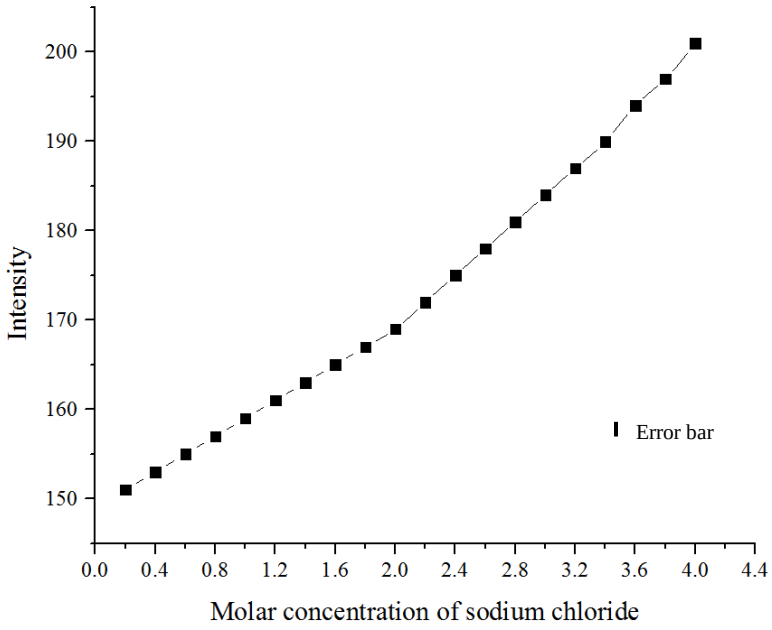

Figure 3.19 Averaged Intensity Values of CMOS Sensor Outputs

3.4.2 Results

From the spectrum of sodium solution obtained by the spectrometer, the intensity of Raman scattering is non-linear to the concentration. From Fig. 3.19, the intensity output of CMOS sensor is non-linear as expected. By comparing the results of the spectrometer and the CMOS image, the concentration of the solution can be detected by this Raman scattering based CMOS imaging system. The averaged value shows that for the lower concentration, the intensity gap between every 0.2 M is smaller than for the high concentration. Figure 3.19 shows that for the averaged output intensity, the concentration of the sodium chloride solution is readable from the plot with a resolution of 0.2 M. However, the real-time output every 8 seconds is not as stable as shown in Figure 3.19. The statistics of the CMOS outputs for each concentration show a maximum deviation of 1.6. For the output every 8 seconds, the resolution is 0.4 M.

This sensor is not able to detect what chemical is in the solution and distinguish a mix of chemicals. It is designed to detect the concentration of a known unique chemical and a mix of known chemicals in a solution for bio-medical applications. With a database of intensity-concentration for the specified chemical, the concentration is readable every 8 seconds. So an overall resolution of detection as 0.4 M for 8 seconds monitoring and 0.2 M resolutions for off-line one-time detection in 2 minutes are reported. By increasing the exposure time of the CMOS sensor, this system is able to reach a resolution higher than 0.2 M.

CHAPTER 4

CONCLUSIONS AND FUTURE DIRESTIONS

4.1 Optical pH Sensor Based on CMOS Contact Imaging and Microfluidics

First, compared to the work of two pieces of fluorescence emission filters cut and glued on a CMOS sensor [17], two identical sensing filters are created with high shape, thickness and response repeatability on the same CMOS sensing array. Second, this work is based entirely on contact imaging techniques, using a CMOS sensor board that makes it more compact than other optical pH sensors based on the electrical diode and spectrometer. This system represents a miniaturized pH detection device, with low power consumption. Furthermore, this device is inexpensive to fabricate and environment-friendly. Also, the sensing components presented in this system are easier to remove, and thus, facilitate reuse of the sensor while the embedded diode system is not reusable. Third, microfluidics is used to enable online monitoring. Fourth, sol-gel deposition and printing methods are optimized so that a thin crack-free sol-gel pattern can be printed without the use of an expensive inkjet and spray machine. Here a repeatable screen-spin printing method that is promising for the successful printing of sol-gel based thin films or patterns is proposed. Fifth, a low-cost compact system that gives accurate measurements of pH values ranging from 4 to 12 by a resolution of 1 in 15 seconds in 20^{o}C to 40^{o}C environments, based on the advantages of contact imaging and sol-gel technology was reported and presented.

4.1.1 Future Work

To broaden the pH detecting range, more than one absorption-based pH indicator can be entrapped into sol-gel and be printed on the same CMOS sensor. More than one substance can also be detected by this system. The method is doping other specific probes for the substance in sol-gel filters.

4.2 Real-Time Biochemical Sensor Based on Raman Scattering with CMOS Contact Imaging

This work presents a qualitative chemical detection sensor for bio-medical solutions. The sensor readings are compared to spectrometer readings by detecting sodium chloride solutions from 0.2 M to 4 M by step of 0.2 M. The amount of Raman scattering photons received by the spectrometer and by the CMOS sensor are the same. The experiment results show a non-linear relation between the concentrations of sodium chloride solution to the total Raman scattering intensity. This relation is confirmed by literature [45-46]. With the database of intensity-concentration for known chemicals solution, this real-time biochemical sensor based on Raman scattering with a CMOS contact imager is able to give the concentration in 8 seconds with a resolution of 0.4 M and in 2 minutes with a resolution of 0.2 M.

4.2.1 Future Work

The downsides of this Raman system is it is not able to detect what chemical is in the solution and distinguish a mix of chemicals, not able to detect the concentration of suspension and microbe, not able to eliminate fluorescence . .To overcome the drawbacks, using two lasers with 3nm shift and a grating or Fourier elements will enable the detection of chemicals is in the solution, the distinguishing of a mix of chemicals and the elimination of fluorescence.

Reference

[1] K. F. Tipton, H. B. F. Dixon, “Effects of pH on enzymes”. *Methods in enzymology*, vol. no. 63, pp. 183-234, 1979.

[2] L. S. Fosdick, Jr. A. C. Starke, “Solubility of Tooth Enamel in Saliva at Various pH Levels”, *Journal of Dental Research*, vol.18, pp. 417-430, 1939.

[3] D. Wencel, T. Abel and C. Mcdonagh, "Optical Chemical pH Sensors", *Analytical Chemistry*, vol. 86, no. 1, pp. 15–29, 2013.

[4] A. Martinez-olmos, S. Capel-cuevas, N.López-ruiz, A. J. Palma, I. De Orbe, and L. F. Capitán-Vallvey, "Sensor Array-Based Optical Portable Instrument for Determination of pH", *Sensors and Actuators B: Chemical*, vol. 156, no. 2, pp. 840–848, 2011.

[5] G. Orellana, "Luminescent Optical Sensors," *Analytical and Bioanalytical Chemistry*, vol. 379, no. 3, pp. 344–346, 2004.

[6] D. Aigner, S.M. Borisov and F.J.O. Fernández, J. F. F. Sánchez, R. Saf, and I. Klimant, "New Fluorescent pH Sensors Based on Covalently Linkable Pet Rhodamines,"*Talanta*, vol. 99, no. 2-3, p. 194, 2012.

[7] Y. Dattner , and O. Yadid-Pecht, "Low-light CMOS Contact Imager with An Integrated Poly-Acrylic Emission Filter for Fluorescence Detection," *Sensors*, vol. 10, issue 5, pp. 5014-5027, 2010.

[8] E. Wang, K.F. Chow, V.Kwan, T. Chin, C. Wong, A. Bocarsly, "Fast and Long Term Optical Sensors for pH Based on Sol–Gels," *Analytica Chimica Acta*, vol. 495, no. 1, pp. 45–50, 2003.

[9] X. Chen and Z. Gu, “Absorption-Type Optical pH Sensitive Film Based on Immobilized Purple Cabbage Pigment”, *Sensors and Actuators B: Chemical*, vol. 178, pp. 207-211, 2013.

[10] A. Yari and M. Dinarvand, "Sol-gel Film Doped with Bromopyrogallol Red as a Highly Sensitive Sensing Element for A New pH Optical Sensor", *Journal of the Iranian Chemical Society*, vol. 8, pp. 1091-1097, 2011.

[11] L. Florea, C. Fay, E. Lahiff, T. Phelan, N. E. O'Connor, B. Corcoran, D. Diamonda and F. Benito-Lopez, "Dynamic pH Mapping in Microfluidic Devices by Integrating Adaptive Coatings Based on Polyaniline with Colorimetric Imaging Techniques", *Lab Chip*, vol. 13, pp. 1079-1085,2013.

[12] I. Gill and A. Ballesteros, "Bioencapsulation within Synthetic Polymers (Part 1): Sol–Gel Encapsulated Biologicals", *Trends in biotechnology*, vol. 18, no.7, pp. 282-296, 2000.

[13] I. Gill and A. Ballesteros, "Bioencapsulation within Synthetic Polymers (Part 2): Non-Sol–Gel Protein–Polymer Biocomposites, *Trends in biotechnology*, vol. 18, no.11, pp. 282-296, 2000.

[14] P. Mintchev, R. J. Turner, and O. Yadid Pecht, "pH Sensor Based on Low-Light Fluorescence Detection for Diagnosis of Gastroesophageal Reflux Disease" in the IEEE Sensors Conference, Baltimore, MD, USA, 5-6 Nov., 2013

[15] L. Blockstein, C. C. Luk, A. K. Mudraboyina, N. I. Syed and O. Yadid-Pecht, "A Pvac-Based Benzophenone-8 Filter as An Alternative to Commercially Available Dichroic Filters for Monitoring Calcium Activity in Live Neurons via Fura-2 AM", *IEEE Photonics Journal*, vol. 4, no. 3, pp. 1004-1012, 2012.

[16] A. K. Mudraboyina, L. Blockstein, C. C. Luk, N. I. Syed and O. Yadid-Pecht, "A Novel Lensless Miniature Contact Imaging System for Monitoring Calcium Changes in Live Neurons", *IEEE Photonics Journal*, vol. 6, no. 1, 2014.

[17] L. Blockstein and O. Yadid-Pecht, “Lensless Miniature Portable Fluorometer for Measurement of Chlorophyll and CDOM in Water Using Fluorescence Contact Imaging”, *IEEE Photonics Journal*, vol. 6, no. 3, pp. 1-16, 2014.

[18] H. Ji, D. Sandar, A. Haas, and P. A. Abshire, “Contact Imaging: Simulation and Experiment”, *IEEE Trans. Circuits System*, vol. 54, no. 8, pp. 1698–1710, Aug, 2007.

[19] C.J. Barbe, D. J. Cassidy, G.Triani, B.A. Latella, D.R.G. Mitchell, K.S. Finnie, K. Short, J.R. Bartlett, J.L. Woolfrey and G.A. Collins, "Sol-Gel Bonding of Silicon Wafers-Part 1: Influence of the Processing Temperature on Final Bond Morphology and Interfacial Energy", *Thin Solid Films*, vol. 488, no. 1-2, pp. 153–159, 2005.

[20] C.J. Barbe, D.J. Cassidy, G.Triani, B.A. Latella, D.R.G. Mitchell, K.S. Finnie, K. Short, J.R. Bartlett, J.L. Woolfrey and G.A. Collins, "Sol-gel Bonding of Silicon Wafers-Part 2. Influence of the Sol–Gel Chemistry on Bond Morphology and Interfacial Energy", *Thin Solid Films*, vol. 488, no. 1, pp. 160–166, 2005.

[21] C.J. Brinker, G.C. Frye, A. J. Hurd and C. S. Ashley, "Fundamentals of Sol-Gel Dip Coating," *Thin Solid Films*, vol. 201, no. 1, pp. 97–108, 1991.

[22] S.A. Ruiz and C.S. Chen, "Microcontact Printing: A Tool to Pattern", *Soft Matter*, vol. 32, pp. 168–177, 2007.

[23] A. Perl, D.N. Reinhoudt and J.Huskens, "Microcontact Printing: Limitations and Achievements", *Advanced Materials*, vol. 2122, pp. 2257–2268, 2009.

[24] S.M. Hossain, R.E. Luckham, A.M. Smith, J. M. Lebert, L. M. Davies, R. H. Pelton, C. D. M. Filipe and J. D. Brennan, "Development of a Bioactive Paper Sensor for Detection of Neurotoxins Using Piezoelectric Inkjet Printing of Sol−Gel-Derived Bioinks", *Analytical Chemistry*, vol. 81, no. 13, pp. 5474–5483, 2009.

[25] R. Hansch, M. R. Chowdhury and N. H. Menzler, "Screen Printing of Sol–Gel-Derived Electrolytes for Solid Oxide Fuel Cell (SOFC) Application", *Ceramics International*, vol. 35, no. 2, pp. 803-811, 2009.

[26] T. Datta-Chaudhuri, P. Abshire and E. Smela, "Packaging Commercial CMOS Chips for Lab on a Chip Integration", *Lab on a Chip*, vol. 14, no. 10, pp. 1753-1766, 2014.

[27] D. Mark, S. Haeberle, G. Roth, F. V. Stetten, R. Zengerle, "Microfluidic Lab-On-A-Chip Platforms: Requirements, Characteristics and Applications", *Chemical Society Reviews*, vol. 39, no. 3, pp. 1153-1182, 2007.

[28] C. Jeffrey Brinker，George W. Scherer, "Sol-Gel Science: The Physics and Chemistry of Sol-Gel Processing", *Academic Press Inc*., pp. 398-401, 506, 1990.

[29] C.J. Brinker, A.J. Hurd, P.R. Schunk, G.C. Frye and C.S. Ashley, "Review of Sol-Gel Thin Film Formation", *Journal of Non-Crystalline Solids*, vol. 147-148, pp. 424-436, 1992.

[30] I. Holowacz, H. Podbielska, J. Bauer, A. Ulatowska-Jarza, "Viscosity, Surface Tension and Refractive Index of Tetraethylorthosilicate-Based Sol-Gel Materials Depending on Ethanol Content", *Optica Applicata*, vol. 35, no. 4, pp. 691-699, 2005.

[31] H. Kozuka, "Stress Evolution on Gel-To-Ceramic Thin Film Conversion", *Journal of Sol-Gel Science and Technology*, vol. 40, no.2, pp. 287-297, 2006.

[32] A.G. Evans, M.D. Drory, and M. S. Hu, "The Cracking and Decohesion of Thin Films", *Journal of materials research*, vol. 3, no. 5, 1988, pp 1043-1049, 1988.

[33] P. P. Kalantri, R. R. Somani, and D. T. Makhija, "Raman Spectroscopy: A Potential Technique in Analysis of Pharmaceuticals", *Der Chemica Sinica*, vol. 1, no. 1, pp. 1-12, 2010.

[34] C. L. Evans, E. O. Potma, M. Puoris' haag, D. Côté, C. P. Lin, and X. S. Xie, "Chemical Imaging of Tissue in Vivo with Video-Rate Coherent Anti-Stokes Raman Scattering Microscopy", *Proceedings of the National Academy of Sciences of the United States of America*, vol. 102, no. 46, pp. 16807-16812, 2005.

[35] E. B. Hanlon, R. Manoharan, T. W. Koo, K. E. Shafer, J. T. Motz, M. Fitzmaurice, J. R. Kramer, I. Itzkan, R. R. Dasari, and M. S. Feld, "Prospects for in Vivo Raman spectroscopy," *Physics in Medicine and Biology*, vol. 45, no.2, pp. 1-59, 2000.

[36] I. Nissinen, J. Nissinen, A.-K. Länsman, L. Hallman, A. Kilpelä, J. Kostamovaara, M. Kögler, M. Aikio, and J. Tenhunen, "A Sub-NS Time-Gated CMOS Single-Photon Avalanche Diode Detector for Raman Spectroscopy," in Proceedings of the European Solid-State Device Research Conference (ESSDRERC) , Institute of Electrical and Electronics Engineers, pp. 375–378, 2011.

[37] J. Kostamovaara, J. Tenhunen, M. Kögler, I. Nissinen, J. Nissinen, and P. Keränen, "Fluorescence Suppression in Raman Spectroscopy Using A Time-Gated CMOS SPAD", *Optics Express*, vol. 21, no. 25, pp. 31632-31645, 2013.

[38] K. Gabet, F. Fuest, J. Sutton, "Quantification and Accuracy of a CMOS-Based Raman/Rayleigh Scattering Imaging System for High-Speed Measurements in Flames", in 8th U.S. National Combustion Meeting, Organized by the Western States Section of the Combustion Institute and hosted by the University of Utah May 19-22, 2013.

[39] D. Barron and A.D. Buckingham, "Rayleigh and Raman Scattering from Optically Active Molecules", *Molecular Physics*, vol. 20, no. 6, pp. 1111-1119, 1971.

[40] QE Pro Spectrometer, Ocean Optics, [online] 2015, http://oceanoptics.com/product/qe-pro/ (Accessed: 13 April 2015)

[41] X. Dou, Y. Yamaguchi, H. Yamamoto, S. Doi and Y. Ozaki, "A Highly Sensitive, Compact Raman System without A Spectrometer for Quantitative Analysis of Biological Samples", *Vibrational Spectroscopy*, vol. 14, no. 2, pp. 199–205, 1997.

[42] B. M. Cullum, J. Mobley, Z. Chi, D. L. Stokes, G. H. Miller and T. Vo-Dinh, "Development of a Compact, Handheld Raman Instrument with No Moving Parts For Use in Field Analysis", *Review of Scientific Instruments*, vol. 71, no. 4, pp. 1602-1607, 2000.

[43] I. R. Lewis and H. Edwards, Handbook of Raman Spectroscopy: From the Research Laboratory to the Process Line, Chapter 7, pp. 275-306.

[44] R.A. Litjens, T.I. Quickenden and C.G. Freeman, "Visible and Near-Ultraviolet Absorption Spectrum of Liquid Water", *Applied Optics*, vol. 38, no. 7, pp. 1216–1223, 1999.

[45] M. Baumgartner and R. J. Bakker, "Raman Spectroscopy of Pure H_2O and NaCl-H_2O Containing Synthetic Fluid Inclusions in Quartz—A Study of Polarization Effects", *Mineralogy and Petrology*, vol. 95, no. 1, pp. 1-15, 2009.

[46] K. Furić, I. Ciglenečki, and B. Ćosović, "Raman Spectroscopic Study of Sodium Chloride Water Solutions", *Journal of Molecular Structure*, vol. 550, pp. 225-234, 2000.